

1 **Trends in atmospheric evaporative demand in Great Britain**
2 **using high-resolution meteorological data**

3

4 **Emma L. Robinson¹, Eleanor M. Blyth¹, Douglas B. Clark¹, Jon Finch¹ and Alison**
5 **C. Rudd¹**

6 [1]{Centre for Ecology and Hydrology, Maclean Building, Benson Lane, Crowmarsh Gifford,
7 Wallingford OX10 8BB }

8 Correspondence to: Emma L. Robinson (emrobi@ceh.ac.uk)

9

10 **Abstract**

11 Observations of climate are often available on very different spatial scales from observations
12 of the natural environments and resources that are affected by climate change. In order to help
13 bridge the gap between these scales using modelling, a new dataset of daily meteorological
14 variables was created at 1 km resolution over Great Britain for the years 1961-2012, by
15 interpolating coarser resolution climate data and including the effects of local topography.
16 These variables were used to calculate atmospheric evaporative demand (AED) at the same
17 spatial and temporal resolution. Two functions that represent AED were chosen: one is a
18 standard form of Potential Evapotranspiration (PET) and the other is a derived PET measure
19 used by hydrologists that includes the effect of water intercepted by the canopy (PETI).
20 Temporal trends in these functions were calculated, with PET found to be increasing in all
21 regions, and at an overall rate of $0.021 \pm 0.021 \text{ mm d}^{-1} \text{ decade}^{-1}$ in Great Britain. PETI was found
22 to be increasing at a rate of $0.019 \pm 0.020 \text{ mm d}^{-1} \text{ decade}^{-1}$ in Great Britain, but this was not
23 statistically significant. However, there was a trend in PETI in England of $0.023 \pm 0.023 \text{ mm d}^{-1} \text{ decade}^{-1}$.
24 The trends were found to vary by season, with spring PET increasing by 0.043 ± 0.019
25 $\text{mm d}^{-1} \text{ decade}^{-1}$ ($0.038 \pm 0.018 \text{ mm d}^{-1} \text{ decade}^{-1}$ when the interception correction is included) in
26 Great Britain, while there is no statistically significant trend in other seasons. The trends were
27 attributed analytically to trends in the climate variables; the overall positive trend was
28 predominantly driven by rising air temperature, although rising specific humidity had a negative
29 effect on the trend. Recasting the analysis in terms of relative humidity revealed that the overall
30 effect is that falling relative humidity causes the PET to rise. Increasing downward short- and
31 longwave radiation made an overall positive contribution to the PET trend, while decreasing
32 wind speed made a negative contribution to the trend in PET. The trend in spring PET was
33 particularly strong due to a strong decrease in relative humidity and increase in downward
34 shortwave radiation in the spring.

35

36 **1 Introduction**

37 There are many studies showing the ways in which our living environment is changing over
38 time: changing global temperatures (IPCC, 2013), radiation (Wild, 2009) and wind speeds
39 (McVicar et al., 2012) can have significant impacts on ecosystems and human life (IPCC,
40 2014a). While there are overall global trends, the impacts can vary between regions (IPCC,
41 2014b). In the UK, wildlife surveys of both flora (Wood et al., 2015; Evans et al., 2008) and
42 fauna (Pocock et al., 2015) show a shift in patterns and timing (Thackeray et al., 2010). In
43 addition, the UK natural resources of freshwater (Watts et al., 2015), soils (Reynolds et al.,
44 2013; Bellamy et al., 2005) and vegetation (Berry et al., 2002; Hickling et al., 2006; Norton et
45 al., 2012) are changing. The UK is experiencing new environmental stresses on the land and
46 water systems through changes in temperature and river flows (Crooks and Kay, 2015; Watts
47 et al., 2015; Hannaford, 2015), which are part of a widespread global pattern of temperature
48 increase and circulation changes (Watts et al., 2015).

49 To explain these changes in terms of climate drivers, there are several gridded meteorological
50 datasets available at global and regional scales. Global datasets can be based on observations –
51 for example the 0.5° resolution Climate Research Unit time series 3.21 (CRU TS 3.21) data
52 (Jones and Harris, 2013; Harris et al., 2014) – while some are based on global meteorological
53 reanalyses bias-corrected to observations – for example the WATCH Forcing Data (WFD, 0.5°;
54 Weedon et al. (2011)), the WATCH Forcing Data methodology applied to ERA-Interim
55 reanalysis product (WFDEI, 0.5°; Weedon et al. (2014)) and the Princeton Global
56 Meteorological Forcing Dataset (0.25°–1°; Sheffield et al. (2006)). At the regional scale in
57 Great Britain (GB), there are datasets that are derived directly from observations – for example
58 the Met Office Rainfall and Evaporation Calculation System (MORECS) dataset at 40 km
59 resolution (Thompson et al., 1981; Hough and Jones, 1997; Field, 1983) and the UKCP09
60 observed climate data at 5 km resolution (Jenkins et al., 2008).

61 However, while regional observations of carbon, methane and water emissions from the land
62 (Baldocchi et al., 1996), the vegetation cover (Morton et al., 2011) and soil properties
63 (FAO/IIASA/ISRIC/ISS-CAS/JRC, 2012) are typically made at the finer landscape scale of
64 100 m to 1000 m, most of these long-term gridded meteorological datasets are only available
65 at a relatively coarse resolution of a few tens of km. These spatial scales may not be
66 representative of the climate experienced by the flora and fauna being studied, and it has also
67 been shown that input resolution can have a strong effect on the performance of hydrological

68 models (Kay et al., 2015). In addition, the coarse temporal resolution of some datasets, for
69 example the monthly CRU TS 3.21 data (Harris et al., 2014; Jones and Harris, 2013), can miss
70 important sub-monthly extremes.

71 Regional studies are important to identify drivers and impacts of changing meteorology that
72 may or may not be reflected in trends in global means. For example, in Canada (Vincent et al.,
73 2015) and Europe (Fleig et al., 2015), high resolution meteorological data have been used to
74 identify the impacts of changing circulation patterns, while in Australia wind speed data have
75 been used to quantify the effects of global stilling in the region (McVicar et al., 2008). While
76 there are datasets available at finer spatial and temporal resolutions for the UK (such as
77 UKCP09 (Jenkins et al., 2008)), these often do not provide all the variables needed to identify
78 the impacts of changing climate.

79 To address this, we have created a meteorological dataset for Great Britain at 1 km resolution:
80 the Climate Hydrology and Ecology research Support System meteorology dataset for Great
81 Britain (1961-2012) (CHESS-met; Robinson et al. (2015b)). It is derived from the observation-
82 based MORECS dataset (Thompson et al., 1981; Hough and Jones, 1997), and then downscaled
83 using information about topography. This is augmented by an independent precipitation dataset
84 – Gridded Estimates of daily and monthly Areal Rainfall for the United Kingdom (CEH-GEAR;
85 Tanguy et al. (2014); Keller et al. (2015)) – along with variables from two global datasets –
86 WFD and CRU TS 3.21 – to produce a comprehensive, observation-based, daily meteorological
87 dataset at 1 km × 1 km spatial resolution.

88 In order to understand the effect of meteorology on the water cycle, a key variable in
89 hydrological modelling is the atmospheric evaporative demand (AED), which is determined by
90 meteorological variables (Kay et al., 2013). It has been shown that water-resource and
91 hydrological model results are largely driven by how this property is defined and used
92 (Haddeland et al., 2011). The AED can be expressed in several ways, for instance the
93 evaporation from a wet surface, from a well-watered but dry uniform vegetated cover, or from
94 a hypothetical well-watered but dry version of the actual vegetation. Metrics such as the Palmer
95 Drought Severity Index (PDSI; Palmer (1965)) use potential evapotranspiration (PET) as an
96 input to represent AED, while many hydrological models such as Climate and Land use
97 Scenario Simulation in Catchments (CLASSIC; Crooks and Naden (2007)) or Grid-to-Grid
98 (G2G; Bell et al. (2009)), which also require an input representing AED, use a distinct form of
99 the PET which includes the intercepted water from rainfall (this is described later in the text)

100 which we hereby name PETI. While hydrological models can make use of high resolution
101 topographic information and precipitation datasets, they are often driven with PET calculated
102 at a coarser resolution (Bell et al., 2011; Bell et al., 2012; Kay et al., 2015). Therefore, we have
103 also created a 1 km × 1 km resolution dataset, the Climate Hydrology and Ecology research
104 Support System Potential Evapotranspiration dataset for Great Britain (1961-2012) (CHES-
105 PE; Robinson et al. (2015a)), consisting of estimates of PET and PETI, which can be used to
106 run high-resolution hydrological models.

107 Other regional studies have created gridded estimates of AED in Austria (Haslinger and
108 Bartsch, 2016) and Australia (Donohue et al., 2010). Regional studies of trends in AED have
109 seen varied results, with increasing AED seen in Romania (Paltineanu et al., 2012), Serbia
110 (Gocic and Trajkovic, 2013), Spain (Vicente-Serrano et al., 2014), some regions of China (Li
111 and Zhou, 2014) and Iran (Azizzadeh and Javan, 2015; Hosseinzadeh Talaei et al., 2013; Tabari
112 et al., 2012), decreasing AED in north east India (Jhajharia et al., 2012) and regions in China
113 (Yin et al., 2009; Song, 2010; Shan et al., 2015; Zhao et al., 2015; Zhang et al., 2015; Lu et al.,
114 2016) and regional variability in Australia (Donohue et al., 2010) and China (Li et al., 2015).
115 In order to understand this variability, it is important to quantify the relative contributions of
116 the changing meteorological variables to trends in AED and regional studies often find different
117 drivers of changing AED (see McVicar et al. (2012) for a review). Relative humidity has been
118 shown to drive AED in the Canary Islands (Vicente-Serrano et al., 2016), wind speed and air
119 temperature were shown to have nearly equal but opposite effects in Australia (Donohue et al.,
120 2010), while in China sunshine hours (Li et al., 2015), wind speed (Yin et al., 2009) or a
121 combination of the two (Lu et al., 2016) have been shown to drive trends. Rudd and Kay (2015)
122 investigated projected changes in PET using a regional climate model, but little has been done
123 to investigate historical trends of AED in the UK.

124 The objectives of this paper are (i) to evaluate the trends in key meteorological variables in
125 Great Britain over the years 1961-2012; (ii) to evaluate the AED in Great Britain over the same
126 time period using PET; (iii) to investigate the effect of including interception in the formulation
127 of PET called PETI; (iv) to evaluate trends in PET over the time period of interest; and (v) to
128 attribute the trends in PET to trends in meteorological variables. To address these objectives,
129 the paper is structured as follows. Section 2 presents the calculation of the meteorological
130 variables. Section 3 presents the calculation of PET and PETI from the meteorological variables
131 and assesses the difference between PET and PETI. In Section 4 the trends of the meteorological

132 variables and AED are calculated and the trends in PET are attributed to trends in
133 meteorological variables. In Section 5 the results are discussed and conclusions are presented
134 in Section 6.

135 **2 Calculation of meteorological variables**

136 The meteorological variables included in this new dataset (Robinson et al., 2015b) are daily
137 mean values of air temperature, specific humidity, wind speed, downward longwave (LW) and
138 shortwave (SW) radiation, precipitation and air pressure, plus daily temperature range (Table
139 1). These variables are important drivers of near-surface conditions, and, for instance, are the
140 full set of variables required to drive the JULES land surface model (LSM) (Best et al., 2011;
141 Clark et al., 2011), as well as other LSMs.

142 The data were derived primarily from MORECS, which is a long-term gridded dataset starting
143 in 1961 and updated to the present (Thompson et al., 1981; Hough and Jones, 1997). It
144 interpolates five variables from synoptic stations (daily mean values of air temperature, vapour
145 pressure and wind speed, daily hours of bright sunshine and daily total precipitation) to a 40
146 km × 40 km resolution grid aligned with the Ordnance Survey National Grid. There are
147 currently 270 stations reporting in real time, while a further 170 report the daily readings on a
148 monthly basis, but numbers have varied throughout the run. The algorithm interpolates a
149 varying number of stations (up to nine) for each square, depending on data availability (Hough
150 and Jones, 1997). The interpolation is such that the value in each grid square is the effective
151 measurement of a station positioned at the centre of the square and at the grid square mean
152 elevation, averaged from 00:00 GMT to 00:00 GMT the next day. MORECS is a consistent,
153 quality-controlled time series, which accounts for changing station coverage. The MORECS
154 variables were used to derive the air temperature, specific humidity, wind speed, downward
155 LW and SW radiation and air pressure in the new dataset. The WFD and CRU TS 3.21 datasets
156 were used for surface air pressure and daily temperature range respectively, as they could not
157 be calculated solely from MORECS. Additionally precipitation was obtained from the CEH-
158 GEAR data, which is a product directly interpolated to 1 km from the station data (Keller et al.,
159 2015).

160 The spatial coverage of the dataset was determined by the spatial coverage of MORECS, which
161 covers the majority of Great Britain, but excludes some coastal regions and islands at the 1 km
162 scale. For most of these points, the interpolation was extended from the nearest MORECS

163 squares, but some outlying islands (in particular Shetland and the Scilly Isles) were excluded
164 when the entire island was further than 40 km from the nearest MORECS square.

165 **2.1 Air temperature**

166 Air temperature, T_a (K), was derived from the MORECS air temperature. The MORECS air
167 temperature was reduced to mean sea level, using a lapse rate of -0.006 K m^{-1} (Hough and
168 Jones, 1997). A bicubic spline was used to interpolate from 40 km resolution to 1 km resolution,
169 then the temperatures were adjusted to the elevation of each 1 km square using the same lapse
170 rate. The 1 km resolution elevation data used were aggregated from the Integrated Hydrological
171 Digital Terrain Model (IHDTM) – a 50 m resolution digital terrain model (Morris and Flavin,
172 1990).

173 **2.2 Specific humidity**

174 Specific humidity, q_a (kg kg^{-1}), was derived from the MORECS vapour pressure, e_M (Pa), which
175 was first reduced to mean sea level, using the equation

$$176 \quad e_{sea} = e_M \left(1 - \frac{L_e}{100} h_M \right) \quad (1)$$

177 where L_e is the lapse rate of -0.025 \% m^{-1} and h is the elevation of the MORECS square
178 (Thompson et al., 1981). The actual lapse rate of humidity will, in general, vary according to
179 atmospheric conditions. However, calculating this would require more detailed information
180 than is available in the input data used. Any method of calculating the variation of specific
181 humidity with height will involve several assumptions, but the method used here is well-
182 established and is used by the Met Office in calculating MORECS (Thompson et al., 1981).
183 The value of the vapour pressure lapse rate is chosen to keep relative humidity approximately
184 constant with altitude, rather than assuming that the vapour pressure itself is constant.

185 A bicubic spline was used to interpolate vapour pressure to 1 km resolution then the values
186 were adjusted to the 1 km resolution elevation using the IHDTM elevations and using the same
187 lapse rate, such that

$$188 \quad e = e_{sea,1km} \left(1 + \frac{L_e}{100} h_{1km} \right), \quad (2)$$

189 where $e_{sea,1km}$ is the sea-level vapour pressure at 1 km resolution and h_{1km} is the 1 km resolution
190 elevation.

191 Finally the specific humidity was calculated, using

$$192 \quad q_a = \frac{\epsilon e}{p_* - (1 - \epsilon)e}, \quad (3)$$

193 where e is the vapour pressure (Pa) and $\epsilon = 0.622$ is the mass ratio of water to dry air (Gill,
194 1982). The air pressure, p_* , in this calculation was assumed to have a constant value of 100000
195 Pa because this was prescribed in the computer code. It would be better to use a varying air
196 pressure, as calculated in Section 2.8, but this makes a negligible difference (of a few percent)
197 to the calculated specific humidity and a constant p_* was retained.

198 **2.3 Downward shortwave radiation**

199 Downward SW radiation, S_d (W m^{-2}), was derived from the MORECS hours of bright sunshine
200 (defined as the total number of hours in a day for which solar irradiation exceeds 120 W m^{-2}
201 (WMO, 2013)). The value calculated is the mean SW radiation over 24 hours. The sunshine
202 hours were used to calculate the cloud cover factor, $C_f = n/N$, where n is the number of hours
203 of bright sunshine in a day, and N is the total number of hours between sunrise and sunset
204 (Marthews et al., 2011). The cloud cover factor was interpolated to 1 km resolution using a
205 bicubic spline. The downward SW solar radiation for a horizontal plane at the Earth's surface
206 was then calculated using the solar angle equations of Iqbal (1983) and a form of the Ångström-
207 Prescott equation which relates hours of bright sunshine to solar irradiance (Ångström, 1918;
208 Prescott, 1940), with empirical coefficients calculated by Cowley (1978). They vary spatially
209 and seasonally and effectively account for reduction of irradiance with increasing solar zenith
210 angle, as well as implicitly accounting for spatially- and seasonally-varying aerosol effects.
211 However, they do not vary interannually and thus do not explicitly include long-term trends in
212 aerosol concentration.

213 The downward SW radiation was then corrected for the average inclination and aspect of the
214 surface, assuming that only the direct beam radiation is a function of the inclination and that
215 the diffuse radiation is homogeneous. It was also assumed that the cloud cover is the dominant
216 factor in determining the diffuse fraction (Muneer and Munawwar, 2006). The aspect and
217 inclination were calculated using the IHDTM elevation at 50 m resolution, following the
218 method of Horn (1981), and were then aggregated to 1 km resolution. The top of atmosphere
219 flux for horizontal and inclined surfaces was calculated following Allen et al. (2006) and the
220 ratio used to scale the direct beam radiation.

221 **2.4 Downward longwave radiation**

222 Downward LW radiation, L_d (W m^{-2}), was derived from the 1 km resolution air temperature
223 (Sect. 2.1), vapour pressure (Sect. 2.2) and cloud cover factor (Sect. 2.3). The downward LW
224 radiation for clear sky conditions was calculated as a function of air temperature and
225 precipitable water using the method of Dilley and O'Brien (1998), with precipitable water
226 calculated from air temperature and humidity following Prata (1996). The additional
227 component due to cloud cover was calculated using the equations of Kimball et al. (1982),
228 assuming a constant cloud base height of 1000 m.

229 **2.5 Wind speed**

230 The wind speed at a height of 10 m, u_{10} (m s^{-1}), was derived from the MORECS 10 m wind
231 speed, which were interpolated to 1 km resolution using a bicubic spline and adjusted for
232 topography using a 1 km resolution dataset of mean wind speeds produced by the UK Energy
233 Technology Support Unit (ETSU; Newton and Burch (1985); Burch and Ravenscroft (1992)).
234 This used Numerical Objective Analysis Boundary Layer (NOABL) methodology combined
235 with station wind measurements over the period 1975-84 to produce a map of mean wind speed
236 over the UK. To calculate the topographic correction, the ETSU wind speed was aggregated to
237 40 km resolution, then the difference between each 1 km value and the corresponding 40 km
238 mean found. This difference was added to the interpolated daily wind speed. In cases where
239 this would result in a negative wind speed, the wind speed was set to zero.

240 **2.6 Precipitation**

241 Precipitation rate, P ($\text{kg m}^{-2} \text{s}^{-1}$), is taken from the daily CEH-GEAR dataset (Tanguy et al.,
242 2014; Keller et al., 2015), scaled to the appropriate units. The CEH-GEAR methodology uses
243 natural neighbour interpolation (Gold, 1989) to interpolate synoptic station data to a 1 km
244 resolution gridded daily dataset of the estimated precipitation in 24 hours between 09:00 GMT
245 and 09:00 GMT the next day.

246 **2.7 Daily temperature range**

247 Daily temperature range (DTR), D_T (K), was obtained from the CRU TS 3.21 monthly mean
248 daily temperature range estimates on a 0.5° latitude \times 0.5° longitude grid, which is interpolated
249 from monthly climate observations (Harris et al., 2014; Jones and Harris, 2013). There is no

250 standard way to correct DTR for elevation, so these data were reprojected to the 1 km grid with
251 no interpolation and the monthly mean used to populate the daily values in each month.
252 Although DTR is not required in the calculation of AED, it is a required input of the JULES
253 LSM, in order to run at sub-daily timestep with daily input data.

254 **2.8 Surface air pressure**

255 Surface air pressure, p^* (Pa), was derived from the WFD, an observation-corrected reanalysis
256 product, which provides 3 hourly meteorological data for 1958-2001 on a 0.5° latitude \times 0.5°
257 longitude resolution grid (Weedon et al., 2011). Mean monthly values of WFD surface air
258 pressure and air temperature were calculated for each 0.5° grid box over the years 1961-2001.
259 These were reprojected to the 1 km grid with no interpolation, then the lapse rate of air
260 temperature (Sect. 2.1) used to calculate the integral of the hypsometric equation (Shuttleworth,
261 2012), in order to obtain the air pressure at the elevation of each 1 km grid. The mean monthly
262 values were used to populate the daily values in the full dataset, thus the surface air pressure in
263 the new dataset does not vary interannually, but does vary seasonally. This is reasonable as the
264 trend in surface air pressure in the WFD is negligible (Weedon et al., 2011).

265 **2.9 Spatial and seasonal patterns of meteorological variables**

266 Long-term mean values of the meteorological variables were calculated for each 1 km square
267 over the whole dataset, covering the years 1961-2012 (Fig. 1). Four sub-regions of interest were
268 defined (Fig. 2); three of these regions correspond to nations (England, Wales and Scotland),
269 while the fourth is the ‘English lowlands’, a subset of England, covering south-central and
270 south-east England, East Anglia and the East Midlands (Folland et al., 2015). Mean-monthly
271 climatologies were calculated over the whole of Great Britain (GB), and over these four regions
272 of interest (Fig. 3).

273 The maps clearly show the effect of topography on the variables (Fig. 1), with an inverse
274 correlation between elevation and temperature, specific humidity, downward LW radiation and
275 surface air pressure and a positive correlation with wind speed. The precipitation has an east-
276 west gradient due to prevailing weather systems and orography. The fine-scale structure of the
277 downward SW radiation is due to the aspect and elevation of each grid cell, with more spatial
278 variability in areas with more varying terrain. As no topographic correction has been applied to
279 DTR, it varies only on a larger spatial scale. Although specific humidity is inversely

280 proportional to elevation, relative humidity is not, as the saturated specific humidity will also
281 be inversely proportional to elevation due to the decrease in temperature with height. The strong
282 correlation between wind speed and elevation means that it is very variable over short spatial
283 scales, particularly in Scotland.

284 The mean-monthly climatologies (Fig. 3) demonstrate the differences between the regions, with
285 Scotland generally having lower temperatures and more precipitation than the average, and
286 England (particularly the English lowlands) being warmer and drier.

287 **2.10 Validation of meteorology**

288 The precipitation dataset, CEH-GEAR, has previously been validated against observations
289 (Keller et al., 2015). Other studies discuss the uncertainties in the CRU TS 3.21 daily
290 temperature range data (Harris et al., 2014) and WFDEI air pressure data (Weedon et al., 2014).

291 For the other variables, the MORECS data set is ultimately derived from the synoptic stations
292 around the UK which represent most of the available observed meteorological data for the
293 country. The only way to validate the gridded meteorology presented here is to compare it to
294 independently observed data, which are available at a few sites where meteorological
295 measurement stations that are not part of the synoptic network are located. Here we carry out a
296 validation exercise with data from four sites from the UK, which have meteorological
297 measurements available for between 5 and 10 years. Details of the sites and data are in
298 Appendix A. Fig. 4 shows the comparison of data set air temperature with the observed air
299 temperature at each of the four sites. This shows a strong correlation (r^2 between 0.94 and 0.97)
300 between the data set and the observations. Fig. 5 shows the mean-monthly climatology
301 calculated from both the data set and from the observations (only for times for which
302 observations were available) and demonstrates that the data set successfully captures the
303 seasonal cycle. This has been repeated for downward SW radiation and for an estimate of the
304 mixing ratio of water vapour, 10 m wind speed and surface air pressure (Appendix A). The air
305 temperature, downward SW radiation and mixing ratio all have high correlations and represent
306 the seasonal cycle well. The downward SW is overestimated at Auchencorth Moss, which may
307 be due to local factors (e.g. shading, or the siting of the station within the grid square). The
308 wind speed is overestimated by the derived data set at two sites, which is likely to be due to
309 land cover effects. The modelling which produced the ETSU dataset uses topography but not
310 land cover (Burch and Ravenscroft, 1992; Newton and Burch, 1985), so at sites with tall

311 vegetation the wind speed is likely to be less than the modelled value. The air pressure has a
 312 low correlation because the data set contains a mean-monthly climatological value. However,
 313 the mean bias is low and the RMSE is small, confirming that it is reasonable to use a
 314 climatological value in place of daily data.

315 **3 Calculation of potential evapotranspiration (PET)**

316 There are several ways to assess the evaporative demand of the atmosphere. Pan evaporation
 317 can be modelled using the Pen-Pan model (Rotstayn et al., 2006), or open-water evaporation
 318 can be modelled with the Penman equation (Penman, 1948). However, neither of these account
 319 for the fact that in general the evaporation is occurring from a vegetated surface. A widely used
 320 model is the Penman-Monteith PET, E_P (mm d^{-1} , equivalent to $\text{kg m}^{-2} \text{d}^{-1}$), which is a physically-
 321 based formulation of AED (Monteith, 1965), including the effect of stomatal resistance. It
 322 provides an estimate of AED dependent on the atmospheric conditions but allowing for the fact
 323 that that the water is evaporating through the surface of leaves and thus the resistance is higher.
 324 It can be calculated from the daily meteorological variables using the equation

$$325 \quad E_P = \frac{t_d}{\lambda} \frac{\Delta A + \frac{c_p \rho_a}{r_a} (q_s - q_a)}{\Delta + \gamma \left(1 + \frac{r_s}{r_a}\right)}, \quad (4)$$

326 where $t_d = 86400 \text{ s d}^{-1}$ is the length of a day, $\lambda = 2.5 \times 10^6 \text{ J kg}^{-1}$ is the latent heat of evaporation,
 327 q_s is saturated specific humidity (kg kg^{-1}), Δ is the gradient of saturated specific humidity with
 328 respect to temperature ($\text{kg kg}^{-1} \text{K}^{-1}$), A is the available energy (W m^{-2}), $c_p = 1010 \text{ J kg}^{-1} \text{K}^{-1}$ is the
 329 specific heat capacity of air, ρ_a is the density of air (kg m^{-3}), q_a is specific humidity (kg kg^{-1}),
 330 $\gamma = 0.004 \text{ K}^{-1}$ is the psychrometric constant, r_s is stomatal resistance (s m^{-1}) and r_a is aerodynamic
 331 resistance (s m^{-1}) (Stewart, 1989).

332 The saturated specific humidity, q_s (kg kg^{-1}), is calculated from saturated vapour pressure, e_s
 333 (Pa), using Eq. 3. The saturated vapour pressure is calculated using an empirical fit to air
 334 temperature

$$335 \quad e_s = p_{sp} \exp\left(\sum_{i=1}^4 a_i \left(1 - \frac{T_{sp}}{T_a}\right)^i\right), \quad (5)$$

336 where $p_{sp} = 101325 \text{ Pa}$ is the steam point pressure, $T_{sp} = 373.15 \text{ K}$ is the steam point temperature
 337 and $a = (13.3185, -1.9760, -0.6445, -0.1299)$ are empirical coefficients (Richards, 1971).

338 The derivative of the saturated specific humidity with respect to temperature, Δ ($\text{kg kg}^{-1} \text{K}^{-1}$),
 339 is therefore

$$340 \quad \Delta = \frac{T_{sp}}{T_a^2} \frac{p_* q_s}{p_* - (1-\epsilon)e_s} \sum_{i=1}^4 i a_i \left(1 - \frac{T_{sp}}{T_a}\right)^{i-1}, \quad (6)$$

341 where the air pressure used is the spatially varying air pressure calculated in Sect.2.8.

342 The available energy, A (W m^{-2}), is the energy balance of the surface,

$$343 \quad A = R_n - G, \quad (7)$$

344 where R_n is the net radiation (W m^{-2}) and G is the soil heat flux (W m^{-2}). The net soil heat flux
345 is negligible at the daily timescale (Allen et al., 1998), so the available energy is equal to the
346 net radiation, such that

$$347 \quad A = (1 - \alpha)S_d + \varepsilon(L_d - \sigma T_*^4), \quad (8)$$

348 where σ is the Stefan-Boltzmann constant, α is the albedo and ε the emissivity of the surface
349 and T_* is the surface temperature (Shuttleworth, 2012). For this study the surface temperature
350 is approximated by using the air temperature, T_a .

351 The air density, ρ_a (kg m^{-3}), is a function of air pressure and temperature,

$$352 \quad \rho_a = \frac{p_*}{r T_a}, \quad (9)$$

353 where $r = 287.05 \text{ J kg}^{-1} \text{ K}^{-1}$ is the gas constant of air and the air pressure used is the spatially
354 varying air pressure calculated in Sect. 2.8.

355 The stomatal and aerodynamic resistances are strongly dependent on land cover due to
356 differences in roughness length and physiological constraints on transpiration of different
357 vegetation types. In addition, the albedo and emissivity are also dependent on the land cover.
358 In order to investigate the effect of meteorology on AED, as distinct from land use effects, the
359 PET was calculated for a single land cover type over the whole of the domain. If necessary, this
360 can be adjusted to give an estimate of PET specific to the local land cover, for example using
361 regression relationships (Crooks and Naden, 2007). As a standard, the Food and Agriculture
362 Organization of the United Nations (FAO) calculate reference crop evaporation for a
363 hypothetical reference crop, which corresponds to a well-watered grass (Allen et al., 1998).
364 Following this, the PET in the current study was calculated for a reference crop of 0.12 m
365 height, with constant stomatal resistance, $r_s = 70.0 \text{ s m}^{-1}$, an albedo of 0.23 and emissivity of
366 0.92 over the whole of Great Britain. This study therefore neglects the effect of land-use on
367 evaporation, which could be investigated in future by calculating PET for different land surface
368 types, with different coverage for each year of the dataset.

369 In general, aerodynamic resistance is a function of wind speed and canopy height. Following
 370 Allen et al. (1998), the aerodynamic resistance, r_a ($s\ m^{-1}$), of a reference crop of 0.12 m height
 371 is a function of the 10 m wind speed

$$372 \quad r_a = \frac{278}{u_{10}}. \quad (10)$$

373 Note that, since the wind speed is likely to be biased high at sites with tall vegetation (Sect.
 374 2.10), this implies that the aerodynamic resistance is likely to be biased low, leading to an
 375 overestimate of PET. However, the estimate of PET here is for a reference crop over the whole
 376 of the dataset, and does not consider the effect of tall vegetation, so the wind speed is
 377 appropriate.

378 Thus the PET is a function of six of the meteorological variables: air temperature, specific
 379 humidity, downward LW and SW radiation, wind speed and surface air pressure.

380 To explore the role of the different meteorological variables in the AED, it is helpful to split
 381 the radiative component (the first part of the numerator in Eq. 4) from the wind component (the
 382 second part). Formally, this is defined as follows (Doorenbos, 1977):

383 The radiative component, E_{PR} ,

$$384 \quad E_{PR} = \frac{t_d}{\lambda} \frac{\Delta A}{\Delta + \gamma \left(1 + \frac{r_s}{r_a}\right)}, \quad (11)$$

385 and the aerodynamic component, E_{PA} ,

$$386 \quad E_{PA} = \frac{t_d}{\lambda} \frac{c_p \rho_a (q_s - q_a)}{r_a \left(1 + \frac{r_s}{r_a}\right)}, \quad (12)$$

387 such that $E_P = E_{PR} + E_{PA}$.

388 **3.1 Potential evapotranspiration with interception (PETI)**

389 When rain falls, water is intercepted by the canopy. The evaporation of this water is not
 390 constrained by stomatal resistance but is subject to the same aerodynamic resistance as
 391 transpiration (Shuttleworth, 2012). At the same time, transpiration is inhibited in a wet canopy.
 392 Suppression of transpiration is well observed both by comparing eddy-covariance fluxes and
 393 observations of sap flow (Kume et al., 2006; Moors, 2012), and by observing stomatal and
 394 photosynthesis response to wetting (Ishibashi and Terashima, 1995). For plants which have at
 395 least some of their stomata on the upper surface of the leaves, this can be due to water directly

396 blocking the stomata. However, in GB most plants have stomata only on the underside of the
397 leaves, so the transpiration is inhibited by other mechanisms.

398 Physically, the suppression may be due to the fact that energy is used in evaporating the
399 intercepted water, so less is available for transpiration or that the increased humidity of the air
400 decreases the evaporative demand (Bosveld and Bouten, 2003). It may also be due to the
401 presence of water on the leaf surface causing stomatal closure through physiological reactions,
402 which can be observed even when the stomata are on the underside of a leaf and the water is
403 lying on the upper side (Ishibashi and Terashima, 1995).

404 In the short term after a rain event, potential water losses due to evaporation may be
405 underestimated if only potential transpiration is calculated, and therefore overall rates
406 underestimated. As transpiration is inhibited over the wet fraction of the canopy (Ward and
407 Robinson, 2000), the PET over a grid box will be a linear combination of the potential
408 interception and potential transpiration, each weighted by the fraction of the canopy that is wet
409 or dry. This can be accounted for by introducing an interception term to the calculation of PET,
410 giving PETI. This is modelled as an interception store, which is (partially) filled by rainfall,
411 proportionally inhibiting the transpiration. As the interception store dries, the relative
412 contribution of interception is decreased and the transpiration increases. In this dataset, this
413 correction is applied on days with precipitation, while on days without precipitation the
414 potential is equal to the PET defined in Eq. 4. Although an unconventional definition of PET,
415 a similar interception correction is applied to the PET provided at 40 km resolution by
416 MORECS (Thompson et al., 1981) which is used widely by hydrologists.

417 This method implicitly assumes that the water is liquid, however snow lying on the canopy will
418 also inhibit transpiration, and will be depleted by melting as well as by sublimation. The rates
419 may be slower, and the snow may stay on the canopy for longer than one day. However, the
420 difference of accounting for canopy snow as distinct from canopy water will have a small effect
421 on large-scale averages, as the number of days with snow cover in GB is relatively low, and
422 they occur during winter when the PET is small.

423 The PETI is a weighted sum of the PET, E_P , (as calculated in Eq 2.) and potential interception,
424 E_I , which is calculated by substituting zero stomatal resistance, $r_s=0 \text{ s m}^{-1}$, into Eq. 4. To
425 calculate the relative proportions of interception and transpiration, it is assumed that the wet
426 fraction of the canopy is proportional to the amount of water in the interception store. The

427 interception store, S_I (kg m^{-2}), decreases through the day according to an exponential dry down
 428 (Rutter et al., 1971), such that

$$429 \quad S_I(t) = S_0 e^{-\frac{E_I}{S_{tot}}t}, \quad (13)$$

430 where E_I is the potential interception, S_{tot} is the total capacity of the interception store (kg m^{-2}),
 431 S_0 is the precipitation that is intercepted by the canopy (kg m^{-2}) and t is the time (in days) since
 432 a rain event. The total capacity of the interception store is calculated following Best et al.
 433 (2011), such that

$$434 \quad S_{tot} = 0.5 + 0.05\Lambda, \quad (14)$$

435 where Λ is the leaf area index (LAI). For the FAO standard grass land cover the LAI is 2.88
 436 (Allen et al., 1998). The fraction of precipitation intercepted by the canopy is also found
 437 following Best et al. (2011), assuming that precipitation lasts for an average of 3 hours.

438 The wet fraction of the canopy, C_{wet} , is proportional to the store size, such that

$$439 \quad C_{wet}(t) = \frac{S(t)}{S_{tot}}. \quad (15)$$

440 The total PETI is the sum of the interception from the wet canopy and the transpiration from
 441 the dry canopy,

$$442 \quad E_{PI}(t) = E_I C_{wet}(t) + E_P(1 - C_{wet}(t)). \quad (16)$$

443 This is integrated over one day to find the total PETI, E_{PI} (mm d^{-1}), to be

$$444 \quad E_{PI} = S_0 \left(1 - e^{-\frac{E_I}{S_{tot}}}\right) + E_P \left(1 - \frac{S_0}{E_I} \left(1 - e^{-\frac{E_I}{S_{tot}}}\right)\right). \quad (17)$$

445 This calculation is only carried out for days on which rainfall occurs. On subsequent days it is
 446 assumed that the canopy has sufficiently dried out that the interception component is zero.

447 The PETI is a function of the same six meteorological variables as the PET, plus the
 448 precipitation.

449 **3.2 Spatial and seasonal patterns of PET and PETI**

450 Both PET and PETI have a distinct gradient from low in the north-west to high in the south-
 451 east, and they are both inversely proportional to the elevation (Fig. 6), reflecting the spatial
 452 patterns of the meteorological variables. The PETI is 8 % higher than the PET overall but this

453 difference is larger in the north and west, where precipitation rates, and therefore interception,
454 are higher (Fig. 6). In Scotland, the higher interception and lower AED mean that this increase
455 is a larger proportion of the total, with the mean PETI being 11 % larger than the PET (in some
456 areas the difference is more than 25%). In the English lowlands the difference is smaller, at 6
457 %, but this is a more water limited region where hydrological modelling can be sensitive to
458 even relatively small adjustments to PET (Kay et al., 2013).

459 The seasonal climatology of both PET and PETI follow the meteorology (Fig. 7), with high
460 values in the summer and low in the winter. Although the relative difference peaks in winter,
461 the absolute difference between PET and PETI is bimodal, with a peak in March and a smaller
462 peak in October (September in Scotland) (Fig. 7), because in winter the overall AED is low,
463 while in summer the amount of precipitation is low, so the interception correction is small. The
464 seasonal cycle of PET is driven predominantly by the radiative component, which has a much
465 stronger seasonality than the aerodynamic component (Fig. 8).

466 On a monthly or annual timescale, the ratio of PET to precipitation is an indicator of the wet-
467 or dryness of a region (Oldekop, 1911; Andréassian et al., 2016). Low values of PET relative
468 to precipitation indicate wet regions, where evaporation is demand-limited, while high values
469 indicate dry, water-limited regions. In the wetter regions (Scotland, Wales) mean-monthly PET
470 and PETI (Fig. 7) are on average lower than the mean-monthly precipitation (Fig. 3) throughout
471 the year, while in drier regions (England, English lowlands) the mean PET and PETI are higher
472 than the precipitation for much of the summer, highlighting the regions' susceptibility to
473 hydrological drought (Folland et al., 2015).

474 **4 Decadal trends**

475 **4.1 Meteorological Variables**

476 Annual means of the meteorological variables (Fig. 9) and the PET and PETI (Fig. 10) were
477 calculated for each region. The trends in these annual means were calculated using linear
478 regression; the significance (P value) and 95% confidence intervals (CI) of the slope are
479 calculated specifically allowing for the non-zero lag-1 autocorrelation, to account for possible
480 correlations between adjacent data points (Zwiers and von Storch, 1995; von Storch and Zwiers,
481 1999). The annual trends can be seen in Table 2. In addition, seasonal means were calculated,
482 with the four seasons defined to be Winter (December-February), Spring (March-May),

483 Summer (June-August) and Autumn (September-November), and trends in these means were
484 also found.

485 The trends in the annual and seasonal means for all regions are plotted in Fig. 11; trends that
486 are statistically significant at the 5% level are plotted with solid error bars, those that are not
487 significant are plotted with dashed lines. The analysis was repeated for each pixel in the 1 km
488 resolution dataset; maps of these rates of change can be seen in Fig. B1.

489 There was a statistically significant trend in air temperature in the English Lowlands throughout
490 the year. In the other regions the trends were statistically significant in spring and autumn, and
491 for the annual means. The trends agree with recent trends in the Hadley Centre Central England
492 Temperature (HadCET) dataset (Parker and Horton, 2005) and in temperature records for
493 Scotland (Jenkins et al., 2008) as well as in the CRUTEM4 dataset (Jones et al., 2012). An
494 increase in winter precipitation in Scotland is seen in the current dataset, which leads to a
495 statistically significant increase in the annual mean precipitation of GB. However, all other
496 regions and seasons have no statistically significant trends in precipitation. Long term
497 observations show that there has been little trend in annual precipitation, but a change in
498 seasonality with wetting winters and drying summers since records began, although with little
499 change over the past 50 years (Jenkins et al., 2008). The statistically significant decline in wind
500 speed in all regions is consistent with the results of McVicar et al. (2012) and Vautard et al.
501 (2010), who report decreasing wind speeds in the northern hemisphere over the late 20th
502 century.

503 **4.2 Potential Evapotranspiration**

504 The trends of the meteorological variables are interesting in their own right. But for hydrology,
505 it is the impact that the trends have on evaporation that matters and that depends on their
506 combination, which can be expressed through PET.

507 The regional trends of annual mean PET and PETI and the radiative and aerodynamic
508 components of PET can be seen in Table 2, and the trends in the annual and seasonal means are
509 plotted in Fig. 12 for all regions. Maps of the trends can be seen in Fig. B2. The trend in the
510 radiative component of PET is positive over the whole of GB. However, the trend in the
511 aerodynamic component varies; for much of Wales, Scotland and northern England, it is not
512 significant, or is slightly negative, while in south-east England and north-west Scotland it is
513 positive. This leads to a positive trend in PET over much of GB, but no significant trend in

514 southern Scotland and northern England. There is a statistically significant increase in annual
515 PET in all regions except Wales; the GB trend ($0.021 \pm 0.021 \text{ mm d}^{-1} \text{ decade}^{-1}$) is equivalent to
516 an increase of $0.11 \pm 0.11 \text{ mm d}^{-1}$ ($8.3 \pm 8.1 \%$ of the long term mean) over the whole dataset.
517 Increases in PETI are only statistically significant in England ($0.023 \pm 0.023 \text{ mm d}^{-1} \text{ decade}^{-1}$)
518 and English lowlands ($0.028 \pm 0.025 \text{ mm d}^{-1} \text{ decade}^{-1}$), where the increases over the whole
519 dataset are $0.12 \pm 0.12 \text{ mm d}^{-1}$ ($8.0 \pm 8.0 \%$ of the long term mean) and $0.15 \pm 0.13 \text{ mm d}^{-1}$ (9.7 ± 8.8
520 $\%$ of the long term mean) respectively. There is a difference in trend between different seasons.
521 In winter, summer and autumn there are no statistically significant trends in PET or PETI, other
522 than the English lowlands in autumn, but the spring is markedly different, with very significant
523 trends ($P < 0.0005$) in all regions. The GB spring trends in PET ($0.043 \pm 0.019 \text{ mm d}^{-1} \text{ decade}^{-1}$)
524 and PETI ($0.038 \pm 0.018 \text{ mm d}^{-1} \text{ decade}^{-1}$) are equivalent to an increase of $0.22 \pm 0.10 \text{ mm d}^{-1}$
525 ($13.8 \pm 6.2 \%$ of the long-term spring mean) and $0.20 \pm 0.09 \text{ mm d}^{-1}$ ($11.2 \pm 5.3 \%$ of the long-term
526 spring mean) over the length of the dataset respectively. The radiative component of PET has
527 similarly significant trends in spring, while the aerodynamic component has no significant
528 trends in any season, except the English Lowlands in autumn (Fig. 12).

529 There are few studies of long-term trends in AED in the UK. MORECS provides an estimate
530 of Penman-Monteith PET with interception correction calculated directly from the 40 km
531 resolution meteorological data (Hough and Jones, 1997; Thompson et al., 1981), and increases
532 can be seen over the dataset (Rodda and Marsh, 2011). But as the PET and PETI in the current
533 dataset are ultimately calculated using the same meteorological data (albeit by different
534 methods), it is not unexpected that similar trends should be seen. Site-based studies suggest an
535 increase over recent decades (Burt and Shahgedanova, 1998; Crane and Hudson, 1997), but it
536 is difficult to separate climate-driven trends from local land-use trends. A global review paper
537 (McVicar et al., 2012) identified a trend of decreasing AED in the northern hemisphere, driven
538 by decreasing wind speeds, however they also reported significant local variations on trends in
539 pan evaporation, including the increasing trend observed by Stanhill and Möller (2008) at a site
540 in England after 1968. Matsoukas et al. (2011) identified a statistically significant increase in
541 PET in several regions of the globe, including southern England, between 1983 and 2008,
542 attributing it predominantly to an increase in the radiative component of PET, due to global
543 brightening. However, these results were obtained using reanalysis data, which is limited in its
544 ability to capture trends in wind speed. This limitation has been documented in both northern
545 (Pryor et al., 2009) and southern (McVicar et al., 2008) hemispheres.

546 Regional changes in actual evaporative losses can be estimated indirectly using regional
 547 precipitation and runoff or river flow. Using a combination of observations and modelling,
 548 Marsh and Dixon (2012) identified an increase in evaporative losses in Great Britain from 1961-
 549 2011. Hannaford and Buys (2012) note seasonal and regional differences in trends in observed
 550 river flow, suggesting that decreasing spring flows in the English lowlands are indicative of
 551 increasing AED. However, changing evaporative losses can also be due to changing supply
 552 through precipitation, so it is important to formally attribute the trends in PET to changing
 553 climate, in order to understand changing evapotranspiration.

554 **4.3 Attribution of trends in potential evapotranspiration**

555 In order to attribute changes in PET to changes in climate, the rate of change of PET, dE_p/dt
 556 ($\text{mm d}^{-1} \text{ decade}^{-1}$), can be calculated as a function of the rate of change of each variable
 557 (Roderick et al., 2007),

$$558 \frac{dE_p}{dt} = \frac{dE_p}{dT_a} \frac{dT_a}{dt} + \frac{dE_p}{dq_a} \frac{dq_a}{dt} + \frac{dE_p}{du_{10}} \frac{du_{10}}{dt} + \frac{dE_p}{dL_d} \frac{dL_d}{dt} + \frac{dE_p}{dS_d} \frac{dS_d}{dt} . \quad (18)$$

559 Note that we exclude the surface air pressure, because this dataset uses a mean-monthly
 560 climatology as the interannual variability of air pressure is negligible. The derivative of the PET
 561 with respect to each of the meteorological variables can be found analytically (Appendix C).
 562 The derivatives are calculated from the daily meteorological data at 1 km resolution.
 563 Substituting the slopes of the linear regressions of the gridded annual means (Appendix B) for
 564 the rate of change of each variable with time, and the overall time-average of the derivatives of
 565 PET with respect to the meteorological variables, the contribution of each variable to the rate
 566 of change of PET can be calculated at 1 km resolution. These are then averaged over the regions
 567 of interest. The same can also be applied to the radiative and aerodynamic components
 568 independently.

569 Note that this can also be applied to the regional means of the derivatives of PET and the trends
 570 in the meteorological variables. The results are compared in Table 3 and the two approaches
 571 are consistent. For the regional analysis, we also quote the 95% CI. However, for the gridded
 572 values, there is such high spatial coherence that combining the 95% CI over the region results
 573 in unreasonably constrained results. We therefore use the more conservative CI obtained from
 574 the regional analysis. Also note that this method assumes that the rate of change of the variables
 575 with respect to time is constant over the seasonal cycle (and thus the product of the means is

576 equal to the mean of the products), and indeed this is how it is often applied (Donohue et al.,
577 2010; Lu et al., 2016). The effect of this assumption was investigated by repeating the analysis
578 with seasonal trends and means, but this makes negligible difference to the results.

579 Figure 13 shows the contribution of each meteorological variable to the rate of change of the
580 annual mean PET and to the radiative and aerodynamic components and compares the total
581 attributed trend to that obtained by linear regression. The percentage contribution is in Table 4,
582 calculated as a fraction of the fitted trend. The final column shows the total attributed trend (i.e.
583 the sum of the previous columns) as a percentage of the fitted trend, to demonstrate the success
584 of the attribution at recovering the fitted trends. For the PET trend and for the trend in the
585 radiative component, these values generally sum to the linear regression to within a few percent.
586 However, for the aerodynamic component, the fitted trends are much smaller than the statistical
587 uncertainty. This means that there can be a large and/or negative percentage difference between
588 the attributed and fitted trends, even when the absolute difference is negligible.

589 The largest overall contribution to the rate of change of PET comes from increasing air
590 temperature, which has the effect of increasing the aerodynamic component (as it makes the air
591 more able to hold water), but it decreases the radiative component (due to increasing outgoing
592 LW radiation). Note that in this calculation we are assuming that air temperature and downward
593 LW radiation vary independently, while in reality (and implicit in the calculation of downward
594 LW in Sect. 2.4), downward LW radiation is also proportional to the air temperature so that
595 increases in downward LW broadly cancel the increasing outgoing LW radiation. If we instead
596 used net LW radiation as the independent variable, it is likely that dependence of the rate of
597 change of the radiative component on air temperature would be reduced and compensated by
598 the rate of change of net LW radiation.

599 Overall the next largest increases are caused by increasing downward SW radiation, particularly
600 in the English regions in the spring, as it increases the radiative component of PET. However,
601 in Scotland and Wales, the increasing downward LW radiation is also important. Increasing
602 specific humidity strongly decreases the PET by decreasing the aerodynamic component, while
603 the decreasing wind speed has the effect of increasing the radiative component, but more
604 strongly decreasing the aerodynamic component, so overall it tends to cause a decrease in PET.
605 Since the increasing air temperature and downward LW and SW radiation have the effect of
606 increasing PET, but the increasing specific humidity and decreasing wind speed tend to

607 decrease it, then the overall trend is positive, but smaller than the trend due to air temperature
608 alone.

609 **4.4 Relative humidity**

610 The increase in PET due to increasing air temperature is largely cancelled by the decrease due
611 to increasing specific humidity. However, although we have assumed that specific humidity
612 and air temperature are independent variables, they are in fact coevolving as part of a warming
613 atmosphere. An alternative way of assessing the drivers of AED is to consider relative humidity,
614 R_h , the independent humidity variable. In this case, the PET can be recast in terms of relative
615 humidity, such that

$$616 \quad E_P = \frac{t_d}{\lambda} \frac{\Delta A + \frac{c_p \rho_a}{r_a} q_s (1 - R_h)}{\Delta + \gamma \left(1 + \frac{r_s}{r_a}\right)}. \quad (19)$$

617 Relative humidity can be calculated from the specific humidity using

$$618 \quad R_h = \frac{q_a}{q_s}. \quad (20)$$

619 Although in this case relative humidity is a function of air temperature, through the saturated
620 specific humidity, in reality they are often found to behave as independent variables. It has been
621 shown that there is little cancellation of the air temperature and relative humidity terms when
622 studying both historical data (Vicente-Serrano et al., 2016) and future climate projections
623 (Scheff and Frierson, 2014).

624 The relative humidity annual means, mean-monthly climatology and seasonal trends can be
625 seen in Fig. 14. We find that there is a statistically significant negative trend in relative
626 humidity, in the spring and autumn (except Wales in the autumn) but no overall negative trend
627 in winter or summer, or for the annual means. Maps of the overall mean relative humidity and
628 its trend are in Fig B3. (Jenkins et al., 2008; Dai, 2006)

629 Figure 15 shows the contribution of the different variables to the rate of change of PET with
630 this alternative formulation. The total attributed change is nearly the same as that in Fig. 13,
631 although there are small differences due to statistical uncertainty in the fits. The contribution of
632 air temperature to the rate of change is significantly reduced, so much as to be negligible. It
633 causes the radiative component to decrease as before (due to increased outgoing LW radiation)
634 and the aerodynamic component to decrease (because the rising air temperature increases the
635 saturated specific humidity). Although it is not statistically significant, there is a negative trend

636 in relative humidity, and this leads to an increase in the aerodynamic component, larger than
637 the increase due to increasing downward SW radiation.

638 **5 Discussion**

639 These high resolution datasets provide insight into the effect of the changing climate of Great
640 Britain on AED over the past five decades. There have been significant climatic trends in the
641 UK since 1961; in particular rising air temperature and specific humidity, decreasing wind
642 speed and decreasing cloudiness. Although some are positive and some negative, these
643 meteorological trends combine to give statistically significant trends in PET.

644 Wind speeds have decreased more significantly in the west than the east, and show a consistent
645 decrease across seasons. Contrary to Donohue et al. (2010) and McVicar et al. (2012), this study
646 finds that the change in wind speed of the late 20th and early 21st centuries has not had a
647 dominant influence on PET over the period of study, although it has mitigated the increasing
648 trend in PET. However, the previous studies were concerned with open-water Penman
649 evaporation, which has a simpler (proportional) dependence on wind speed than the Penman-
650 Monteith PET considered here (Schymanski and Or, 2015).

651 The air temperature trend in this study of 0.21 ± 0.15 K decade⁻¹ in GB is consistent with
652 observed global and regional trends (Hartmann et al., 2013; Jenkins et al., 2008). The
653 temperature trend is responsible for a large contribution to the trend in PET, although the large
654 negative contribution from the specific humidity (as well as a small negative contribution from
655 wind speed) means that the overall trend is smaller than the temperature trend alone.

656 When the attribution is recast in terms of relative humidity, the effect of air temperature is
657 negligible, supporting the hypothesis that the temperature and specific humidity components
658 cancel because their changes are part of the same thermodynamic warming processes. However,
659 although the relative humidity does not have a statistically significant trend (except in spring
660 and for some regions in autumn), it is large enough that the negative trend in relative humidity
661 is the largest contribution to the increasing PET, followed by the downward SW radiation.

662 The trend in relative humidity is consistent with that seen in historical regional (Jenkins et al.,
663 2008) and global (Dai, 2006; Willett et al., 2014) analyses. Although not statistically significant
664 overall, it contributes to between 57 % and 68 % of the trends in PET (between 39 % and 46 %
665 or the trends in spring PET). Globally trends in relative humidity vary spatially, with mid-
666 latitudes showing a decrease and the tropics and high-latitudes showing an increase, despite an

667 overall increase in specific humidity over land particularly in the Northern Hemisphere (Dai,
668 2006; Willett et al., 2014). In these global analyses, Great Britain is in a region of transition
669 between decreasing relative humidity in Western Europe and increasing relative humidity in
670 Scandinavia, so that small decreasing trends are found, but they are not significant; this is
671 consistent with our findings. We have found the relative humidity to be decreasing significantly
672 in spring, when the downward SW is increasing. This is again consistent with reduced
673 precipitation and cloud cover due to changing weather patterns (Sutton and Dong, 2012).

674 Increasing solar radiation has been shown to increase spring and annual AED, contributing to
675 between 18 % and 50 % of the fitted trend in annual PET, and to between 43 % and 53 % of
676 the fitted trend in spring PET. Two main mechanisms can be responsible for changing solar
677 radiation – changing cloud cover and changing aerosol concentrations. Changing aerosol
678 emissions have been shown to have had a significant effect on solar radiation in the 20th century.
679 In Europe, global dimming due to increased aerosol concentrations peaked around 1980,
680 followed by global brightening as aerosol concentrations decreased (Wild, 2009). Observations
681 of changing continental runoff and river flow in Europe over the 20th century have been
682 attributed to changing aerosol concentrations, via their effect on solar radiation, and thus AED
683 (Gedney et al., 2014).

684 In this study we use the duration of bright sunshine to calculate the solar radiation, using
685 empirical coefficients which do not vary with year, so aerosol effects are not explicitly included.
686 The coefficients used in this study to convert sunshine hours to radiation fluxes were
687 empirically derived in 1978; the derivation used data from the decade 1966-75, as this period
688 was identified to be before reductions in aerosol emissions had begun to significantly alter
689 observed solar radiation (Cowley, 1978). Despite this, the trend in SW radiation in the current
690 dataset from 1979 onwards ($1.4 \pm 1.4 \text{ W m}^{-2} \text{ decade}^{-1}$) is consistent, within uncertainties, with
691 that seen over GB in the WFDEI data ($0.9 \pm 1.1 \text{ W m}^{-2} \text{ decade}^{-1}$), which is bias-corrected to
692 observations and includes explicit aerosol effects (Weedon et al., 2014).

693 It has been suggested that aerosol effects also implicitly affect sunshine duration since in
694 polluted areas, there will be fewer hours above the official ‘sunshine hours’ threshold of 120
695 Wm^{-2} (Helmes and Jaenicke, 1986). Several regional studies have shown trends in sunshine
696 hours that are consistent with the periods of dimming and brightening across the globe (eg
697 Liley, 2009; Sanchez-Lorenzo et al., 2009; Sanchez-Lorenzo et al., 2008; Stanhill and Cohen,
698 2005), and several have attempted to quantify the relative contribution of trends in cloud cover

699 and aerosol loading (e.g. Sanchez-Lorenzo and Wild (2012) in Switzerland, see Sanchez-
700 Romero et al. (2014) for a review). Therefore, it may be that some of the brightening trend seen
701 in the current dataset is due to the implicit signal of aerosol trends in the MORECS sunshine
702 duration, although this is likely to be small compared to the effects of changing cloud cover.

703 The trends in the MORECS sunshine duration used in this study are consistent with changing
704 weather patterns which may be attributed to the Atlantic Multidecadal Oscillation (AMO). The
705 AMO has been shown to cause a decrease in spring precipitation (and therefore cloud cover) in
706 northern Europe over recent decades (Sutton and Dong, 2012), and the trend in MORECS
707 sunshine hours is dominated by an increase in the spring mean. This has also been seen in
708 Europe-wide sunshine hours data (Sanchez-Lorenzo et al., 2008). On the other hand, the effect
709 of changing aerosols on sunshine hours is expected to be largest in the winter (Sanchez-Lorenzo
710 et al., 2008). However, it would not be possible to directly identify either of these effects on the
711 sunshine duration without access to longer data records.

712 The inclusion of explicit aerosol effects in the coefficients of the Ångström-Prescott equation
713 would be expected to reduce the positive trend in AED in the first two decades of the dataset,
714 and increase it after 1980. Gedney et al. (2014) attribute a decrease in European solar radiation
715 of 10 W m^{-2} between the periods 1901-10 and 1974-80, and an increase of 4 W m^{-2} from 1974-
716 84 to 1990-99 to changing aerosol contributions. Applying these trends to the current dataset,
717 with a turning point at 1980, would double the overall increase in solar radiation in Great
718 Britain, which would lead to a 40 % increase in the overall trend in PET. So, if this effect were
719 to be included, it would confirm the results found in this paper.

720 (Willett et al., 2014; Dai, 2006; Sutton and Dong, 2012) Although the contribution is generally
721 smaller (except in Scotland), the trends in LW radiation in these datasets contribute to between
722 15% and 28% of the trends in PET and between 27% and 46% of the trends in the radiative
723 component. In Scotland the downward LW radiation is the dominant driver of changing PET.
724 Observations of LW radiation are often uncertain, but the trend in this dataset, although small,
725 is consistent with observed trends (Wang and Liang, 2009), as well as with trends in the WFDEI
726 bias-corrected reanalysis product (Weedon et al., 2014).

727 Trends in temperature and cloud cover in the UK are expected to continue into the coming
728 decades, with precipitation expected to increase in the winter but decrease in the summer
729 (Murphy et al., 2009). Therefore it is likely that AED will increase, increasing water stress in
730 the summer when precipitation is lower and potentially affecting water resources, agriculture

731 and biodiversity. This has been demonstrated for southern England and Wales by Rudd and
732 Kay (2015), who calculated present and future PET using high-resolution RCM output and
733 included the effects of CO₂ on stomatal opening.

734 The current study is concerned only with the effects of changing climate on AED and has
735 assumed a constant bulk canopy resistance throughout. However, plants are expected to react
736 to increased CO₂ in the atmosphere by closing stomata and limiting the exchange of gases,
737 including water (Kruijt et al., 2008), and observed changes in runoff have been attributed to this
738 effect (Gedney et al., 2006; Gedney et al., 2014). It is possible that the resulting change of
739 canopy resistance could partially offset the increased atmospheric demand (Rudd and Kay,
740 2015) and may impact runoff (Gedney et al., 2006; Prudhomme et al., 2014), but further studies
741 would be required to quantify this.

742 **6 Conclusion**

743 This paper has presented a unique, high-resolution, observation-based dataset of meteorological
744 variables and AED in Great Britain since 1961. Key trends in the meteorological variables are
745 (i) increasing air temperature and specific humidity, consistent with global temperature trends;
746 (ii) increasing solar radiation, particularly in the spring, consistent with changes in aerosol
747 emissions and weather patterns in recent decades; (iii) decreasing wind speed, consistent with
748 observations of global stilling; and (iv) increasing precipitation, driven by increasing winter
749 precipitation in Scotland. The meteorological variables were used to evaluate AED in Great
750 Britain via calculation of PET and PETI. It has been demonstrated that including the
751 interception component in the calculation of PETI gives a mean estimate that is overall 8%
752 larger than PET alone, with strong seasonality and spatial variation of the difference. PET was
753 found to be increasing by 0.021 ± 0.021 mm d⁻¹ decade⁻¹ in GB over the study period. With the
754 interception component included, the trend in PETI is weaker (0.019 ± 0.020 mm d⁻¹), and over
755 GB is not significant at the 5% level. The trend in PET was analytically attributed to the trends
756 in the meteorological variables, and it was found that the dominant effect was that increasing
757 air temperature was driving increasing PET, with smaller increases from increased downward
758 SW and LW radiation. However, the effect of temperature is largely compensated by the
759 associated increase in specific humidity, while decreasing wind speed tended to decrease the
760 PET. When the attribution was recast in terms of relative humidity, temperature was found to
761 have a negligible effect on the trend in PET, while the decreasing relative humidity caused PET
762 to increase, at a similar rate to the downward SW radiation (and downward LW radiation in

763 Scotland). The increase in PET due to these variables is mitigated by the observed northern
764 hemisphere wind stilling, which causes a decrease in PET, however, the overall trend in PET is
765 positive over the period of study.

766 In addition to providing meteorological data and estimates of AED for analysis, the
767 meteorological variables provided are sufficient to run LSMs and hydrological models. The
768 high spatial (1 km) and temporal (daily) resolution will allow this dataset to be used to study
769 the effects of climate on physical and biological systems at a range of scales, from local to
770 national.

771 **Data Access**

772 The data can be downloaded from the Environmental Information Platform at the Centre for
773 Ecology & Hydrology. The meteorological variables (CHESS-met) can be found at
774 <https://catalogue.ceh.ac.uk/documents/80887755-1426-4dab-a4a6-250919d5020c>,
775 while the PET and PETI (CHESS-PE) can be accessed at
776 <https://catalogue.ceh.ac.uk/documents/d329f4d6-95ba-4134-b77a-a377e0755653>.

777 **Author contribution**

778 EB, JF and DBC designed the study. JF, ACR, DBC and ELR developed code to create
779 meteorological data. ELR created the PET and PETI. ELR and EB analysed trends. ELR, EB,
780 ACR and DBC wrote the manuscript.

781 **Acknowledgements**

782 The meteorological variables presented are based largely on GB meteorological data under
783 licence from the Met Office, and those organisations contributing to this national dataset
784 (including the Met Office, Environment Agency, Scottish Environment Protection Agency
785 (SEPA) and Natural Resources Wales) are gratefully acknowledged. The CRU TS 3.21 daily
786 temperature range data were created by the University of East Anglia Climatic Research Unit,
787 and the WFD air pressure data were created as part of the EU FP6 project WATCH (Contract
788 036946). Collection of flux data was funded by EU FP4 EuroFlux (Griffin Forest); EU FP5
789 CarboEuroFlux (Griffin Forest); EU FP5 GreenGrass (Easter Bush); EU FP6 CarboEuropeIP
790 (Alice Holt , Griffin Forest, Auchencorth Moss, Easter Bush); EU FP6 IMECC (Griffin
791 Forest); the Forestry Commission (Alice Holt); the Natural Environment Research Council,
792 UK (Auchencorth Moss, Easter Bush).

793 Fig. 1 and panels a) and b) of Fig. 6 were produced with the python implementation of the
794 cubehelix colour scheme (Green, 2011).
795 Thanks to Nicola Gedney and Graham Weedon for useful discussions.
796 Thanks to three anonymous reviewers, who provided insightful and helpful comments.
797 This work was partially funded by the Natural Environment Research Council in the
798 Changing Water Cycle programme: NERC Reference: NE/I006087/1.
799

800 **Appendix A: Data validation**

801 Meteorological data were downloaded from the European Fluxes Database Cluster
802 (<http://gaia.agraria.unitus.it>) for four sites positioned around Great Britain. Two were woodland
803 sites (Alice Holt (Wilkinson et al., 2012; Heinemeyer et al., 2012) and Griffin Forest (Clement,
804 2003)), while two had grass and crop cover (Auchencorth Moss (Billett et al., 2004) and Easter
805 Bush (Gilmanov et al., 2007; Soussana et al., 2007)). Table A1 gives details of the data used.
806 The data are provided as half-hourly measurements, which were used to create daily means,
807 where full daily data coverage was available. The daily means of the observed data were
808 compared to the daily data from the grid square containing the site and the Pearson correlation
809 (r^2), mean bias and root mean square error (RMSE) were calculated. For each site, monthly
810 means were calculated where the full month had available data, then a climatology calculated
811 from available months. The same values were calculated from the relevant grid squares, using
812 only time periods for which observed data were available.

813 Fig. A1 shows the comparison of the data set downward SW radiation against daily mean air
814 temperature observed at the four sites. Fig. A2 shows the mean-monthly climatology of the
815 daily values. The observed values of the mixing ratio of water vapour in air were compared
816 with values calculated from the meteorological dataset, using the equation

$$817 \quad r_w = q_a \left(\frac{m_a}{m_w} \right) \quad (\text{A1})$$

818 where m_a is the molecular mass of dry air and m_w is the molecular mass of water. The
819 comparisons are shown in Figs. A3 and A4.

820 Table A2 shows the r^2 , mean bias and RMSE for each of the variables included in the validation
821 exercise. The correlations indicate a good relationship between the dataset variables and the
822 independent observations at the sites, while the mean-monthly climatologies demonstrate that
823 the data represent the seasonal cycle well. The data set downward SW in Auchencorth Moss is
824 biased high compared to the observations, while the wind speed is biased high at two sites.

825 **Appendix B: Trend maps**

826 Fig. B1 shows the rate of change of each of the meteorological variables at the 1 km resolution,
827 while Fig. B2 shows the rate of change of the PET, PETI, and the two components of PET at
828 the same resolution. This shows that the regional trends are consistent with spatial variation and
829 are not dominated by individual extreme points.

830 **Appendix C: Derivatives of PET**

831 The wind speed affects the PET through the aerodynamic resistance. The derivative with respect
832 to wind speed is

$$833 \quad \frac{\partial E_P}{\partial u_{10}} = \frac{(\Delta + \gamma)E_{PA} - \gamma \frac{T_s}{r_a} E_{PR}}{u_{10} \left(\Delta + \gamma \left(1 + \frac{r_s}{r_a} \right) \right)}. \quad (C1)$$

834 The downward LW and SW radiation affect PET through the net radiation, and the derivatives
835 are

$$836 \quad \frac{\partial E_P}{\partial L_d} = E_{PR} \frac{\epsilon}{R_n} \quad (C2)$$

$$837 \quad \frac{\partial E_P}{\partial S_d} = E_{PR} \frac{(1 - \alpha)}{R_n}. \quad (C3)$$

838 The derivative of PET with respect to specific humidity is

$$839 \quad \frac{\partial E_P}{\partial q_a} = \frac{E_{PA}}{q_a - q_s}. \quad (C4)$$

840 The air temperature affects PET through the saturated specific humidity and its derivative, the
841 net radiation and the air density, so that the derivative of PET with respect to air temperature is

$$842 \quad \frac{\partial E_P}{\partial T_a} = E_{PR} \left[\left(1 - \frac{\Delta}{\Delta + \gamma \left(1 + \frac{r_s}{r_a} \right)} \right) \left(\frac{T_{sp}}{T_a^2} \frac{\sum_{i=1}^4 i(i-1) a_i T_r^{i-2}}{\sum_{i=1}^4 i a_i T_r^{i-1}} + \Delta \frac{p_* + (1 - \epsilon) e_s}{p_* q_s} - \frac{2}{T_a} \right) - \frac{4 \epsilon \sigma T_a^3}{R_n} \right] +$$

$$843 \quad E_{PA} \left[\frac{\Delta}{q_s - q_a} - \frac{1}{T_a} - \frac{\Delta}{\Delta + \gamma \left(1 + \frac{r_s}{r_a} \right)} \left(\frac{T_{sp}}{T_a^2} \frac{\sum_{i=1}^4 i(i-1) a_i T_r^{i-2}}{\sum_{i=1}^4 i a_i T_r^{i-1}} + \Delta \frac{p_* + (1 - \epsilon) e_s}{p_* q_s} - \frac{2}{T_a} \right) \right]. \quad (C5)$$

844 When calculating the attribution with relative humidity as the dependent variable, the derivative
845 of PET with respect to relative humidity is

$$846 \quad \frac{\partial E_P}{\partial R_h} = \frac{E_{PA}}{R_h - 1}, \quad (C6)$$

847 and the derivative of PET with respect to air temperature is

$$848 \quad \frac{\partial E_P}{\partial T_a} = E_{PR} \left[\left(1 - \frac{\Delta}{\Delta + \gamma \left(1 + \frac{r_s}{r_a} \right)} \right) \left(\frac{T_{sp}}{T_a^2} \frac{\sum_{i=1}^4 i(i-1) a_i T_r^{i-2}}{\sum_{i=1}^4 i a_i T_r^{i-1}} + \Delta \frac{p_* + (1 - \epsilon) e_s}{p_* q_s} - \frac{2}{T_a} \right) - \frac{4 \epsilon \sigma T_a^3}{R_n} \right] +$$

$$849 \quad E_{PA} \left[\frac{\Delta}{q_s} - \frac{1}{T_a} - \frac{\Delta}{\Delta + \gamma \left(1 + \frac{r_s}{r_a} \right)} \left(\frac{T_{sp}}{T_a^2} \frac{\sum_{i=1}^4 i(i-1) a_i T_r^{i-2}}{\sum_{i=1}^4 i a_i T_r^{i-1}} + \Delta \frac{p_* + (1 - \epsilon) e_s}{p_* q_s} - \frac{2}{T_a} \right) \right]. \quad (C7)$$

850 The difference between Eq. C7 and Eq. C5 is the factor of Δ/q_s instead of $\Delta/(q_s - q_a)$ in the
851 second bracket.

852 7 References

- 853 Allen, R. G., Pereira, L. S., Raes, D., and Smith, M.: Crop evapotranspiration - Guidelines for
854 computing crop water requirements, Food and Agriculture Organization of the United
855 Nations, Rome, Italy, FAO Irrigation and Drainage Paper, 1998.
- 856 Allen, R. G., Trezza, R., and Tasumi, M.: Analytical integrated functions for daily solar
857 radiation on slopes, *Agr Forest Meteorol*, 139, 55-73, doi:10.1016/j.agrformet.2006.05.012,
858 2006.
- 859 Andréassian, V., Mander, Ü., and Pae, T.: The Budyko hypothesis before Budyko: The
860 hydrological legacy of Evald Oldekop, *Journal of Hydrology*, 535, 386-391,
861 <http://dx.doi.org/10.1016/j.jhydrol.2016.02.002>, 2016.
- 862 Ångström, A.: A study of the radiation of the atmosphere, *Smithsonian Miscellaneous*
863 *Collections*, 65, 159-161, 1918.
- 864 Azizzadeh, M., and Javan, K.: Analyzing Trends in Reference Evapotranspiration in
865 Northwest Part of Iran, *Journal of Ecological Engineering*, 16, 1-12,
866 10.12911/22998993/1853, 2015.
- 867 Baldocchi, D., Valentini, R., Running, S., Oechel, W., and Dahlman, R.: Strategies for
868 measuring and modelling carbon dioxide and water vapour fluxes over terrestrial ecosystems,
869 *Global Change Biology*, 2, 159-168, doi:10.1111/j.1365-2486.1996.tb00069.x, 1996.
- 870 Bell, V. A., Kay, A. L., Jones, R. G., Moore, R. J., and Reynard, N. S.: Use of soil data in a
871 grid-based hydrological model to estimate spatial variation in changing flood risk across the
872 UK, *Journal of Hydrology*, 377, 335-350, doi:10.1016/j.jhydrol.2009.08.031, 2009.
- 873 Bell, V. A., Gedney, N., Kay, A. L., Smith, R. N. B., Jones, R. G., and Moore, R. J.:
874 Estimating Potential Evaporation from Vegetated Surfaces for Water Management Impact
875 Assessments Using Climate Model Output, *Journal of Hydrometeorology*, 12, 1127-1136,
876 doi:10.1175/2011jhm1379.1, 2011.
- 877 Bell, V. A., Kay, A. L., Cole, S. J., Jones, R. G., Moore, R. J., and Reynard, N. S.: How might
878 climate change affect river flows across the Thames Basin? An area-wide analysis using the
879 UKCP09 Regional Climate Model ensemble, *Journal of Hydrology*, 442-443, 89-104,
880 doi:10.1016/j.jhydrol.2012.04.001, 2012.
- 881 Bellamy, P. H., Loveland, P. J., Bradley, R. I., Lark, R. M., and Kirk, G. J.: Carbon losses
882 from all soils across England and Wales 1978-2003, *Nature*, 437, 245-248,
883 doi:10.1038/nature04038, 2005.
- 884 Berry, P. M., Dawson, T. P., Harrison, P. A., and Pearson, R. G.: Modelling potential impacts
885 of climate change on the bioclimatic envelope of species in Britain and Ireland, *Global Ecol*
886 *Biogeogr*, 11, 453-462, doi:10.1046/j.1466-822x.2002.00304.x, 2002.
- 887 Best, M. J., Pryor, M., Clark, D. B., Rooney, G. G., Essery, R. L. H., Ménard, C. B., Edwards,
888 J. M., Hendry, M. A., Porson, A., Gedney, N., Mercado, L. M., Sitch, S., Blyth, E., Boucher,
889 O., Cox, P. M., Grimmond, C. S. B., and Harding, R. J.: The Joint UK Land Environment
890 Simulator (JULES), model description – Part 1: Energy and water fluxes, *Geoscientific Model*
891 *Development*, 4, 677-699, doi:10.5194/gmd-4-677-2011, 2011.
- 892 Billett, M. F., Palmer, S. M., Hope, D., Deacon, C., Storeton-West, R., Hargreaves, K. J.,
893 Flechard, C., and Fowler, D.: Linking land-atmosphere-stream carbon fluxes in a lowland
894 peatland system, *Global Biogeochemical Cycles*, 18, n/a-n/a, 10.1029/2003gb002058, 2004.

895 Bosveld, F. C., and Bouten, W.: Evaluating a Model of Evaporation and Transpiration with
896 Observations in a Partially Wet Douglas-Fir Forest, *Boundary-Layer Meteorology*, 108, 365-
897 396, 10.1023/a:1024148707239, 2003.

898 Burch, S. F., and Ravenscroft, F.: Computer modelling of the UK wind energy resource: Final
899 overview report., AEA Industrial Technology, 1992.

900 Burt, T. P., and Shahgedanova, M.: An historical record of evaporation losses since 1815
901 calculated using long-term observations from the Radcliffe Meteorological Station, Oxford,
902 England, *Journal of Hydrology*, 205, 101-111, doi:10.1016/S0022-1694(97)00143-1, 1998.

903 Clark, D. B., Mercado, L. M., Sitch, S., Jones, C. D., Gedney, N., Best, M. J., Pryor, M.,
904 Rooney, G. G., Essery, R. L. H., Blyth, E., Boucher, O., Harding, R. J., Huntingford, C., and
905 Cox, P. M.: The Joint UK Land Environment Simulator (JULES), model description – Part 2:
906 Carbon fluxes and vegetation dynamics, *Geoscientific Model Development*, 4, 701-722,
907 doi:10.5194/gmd-4-701-2011, 2011.

908 Clement, R. M., J.B.; Jarvis, P.G.: Net carbon productivity of Sitka Spruce forest in Scotland,
909 *Scottish Forestry*, 5-10, 2003.

910 Cowley, J. P.: The distribution over Great Britain of global solar irradiation on a horizontal
911 surface, *Meteorological Magazine*, 107, 357-372, 1978.

912 Crane, S. B., and Hudson, J. A.: The impact of site factors and climate variability on the
913 calculation of potential evaporation at Moel Cynnedd, Plynlimon, *Hydrol. Earth Syst. Sci.*, 1,
914 429-445, doi:10.5194/hess-1-429-1997, 1997.

915 Crooks, S. M., and Naden, P. S.: CLASSIC: a semi-distributed rainfall-runoff modelling
916 system, *Hydrol. Earth Syst. Sci.*, 11, 516-531, doi:10.5194/hess-11-516-2007, 2007.

917 Crooks, S. M., and Kay, A. L.: Simulation of river flow in the Thames over 120 years:
918 Evidence of change in rainfall-runoff response?, *Journal of Hydrology: Regional Studies*, 4,
919 Part B, 172-195, doi:10.1016/j.ejrh.2015.05.014, 2015.

920 Dai, A.: Recent Climatology, Variability, and Trends in Global Surface Humidity, *Journal of*
921 *Climate*, 19, 3589-3606, doi:10.1175/JCLI3816.1, 2006.

922 Dilley, A. C., and O'Brien, D. M.: Estimating downward clear sky long-wave irradiance at the
923 surface from screen temperature and precipitable water, *Quarterly Journal of the Royal*
924 *Meteorological Society*, 124, 1391-1401, doi:10.1256/Smsqj.54902, 1998.

925 Donohue, R. J., McVicar, T. R., and Roderick, M. L.: Assessing the ability of potential
926 evaporation formulations to capture the dynamics in evaporative demand within a changing
927 climate, *Journal of Hydrology*, 386, 186-197, doi:10.1016/j.jhydrol.2010.03.020, 2010.

928 Doorenbos, J. a. P., W. O.: Crop water requirements. FAO Irrigation and Drainage Paper 24.,
929 FAO, Rome, Italy, 1977.

930 Evans, N., Baierl, A., Semenov, M. A., Gladders, P., and Fitt, B. D.: Range and severity of a
931 plant disease increased by global warming, *Journal of the Royal Society, Interface / the Royal*
932 *Society*, 5, 525-531, doi:10.1098/rsif.2007.1136, 2008.

933 FAO/IIASA/ISRIC/ISS-CAS/JRC: Harmonized World Soil Database, 2012.

934 Field, M.: The meteorological office rainfall and evaporation calculation system —
935 MORECS, *Agricultural Water Management*, 6, 297-306, [http://dx.doi.org/10.1016/0378-](http://dx.doi.org/10.1016/0378-3774(83)90017-3)
936 [3774\(83\)90017-3](http://dx.doi.org/10.1016/0378-3774(83)90017-3), 1983.

- 937 Fleig, A. K., Tallaksen, L. M., James, P., Hisdal, H., and Stahl, K.: Attribution of European
938 precipitation and temperature trends to changes in synoptic circulation, *Hydrology and Earth
939 System Sciences*, 19, 3093-3107, 10.5194/hess-19-3093-2015, 2015.
- 940 Folland, C. K., Hannaford, J., Bloomfield, J. P., Kendon, M., Svensson, C., Marchant, B. P.,
941 Prior, J., and Wallace, E.: Multi-annual droughts in the English Lowlands: a review of their
942 characteristics and climate drivers in the winter half-year, *Hydrology and Earth System
943 Sciences*, 19, 2353-2375, doi:10.5194/hess-19-2353-2015, 2015.
- 944 Gedney, N., Cox, P. M., Betts, R. A., Boucher, O., Huntingford, C., and Stott, P. A.:
945 Detection of a direct carbon dioxide effect in continental river runoff records, *Nature*, 439,
946 835-838, doi:10.1038/nature04504, 2006.
- 947 Gedney, N., Huntingford, C., Weedon, G. P., Bellouin, N., Boucher, O., and Cox, P. M.:
948 Detection of solar dimming and brightening effects on Northern Hemisphere river flow,
949 *Nature Geoscience*, 7, 796-800, doi:10.1038/ngeo2263, 2014.
- 950 Gill, A. E.: *Atmosphere-ocean Dynamics*, Academic Press, San Diego, California, USA,
951 1982.
- 952 Gilmanov, T. G., Soussana, J. F., Aires, L., Allard, V., Ammann, C., Balzarolo, M., Barcza,
953 Z., Bernhofer, C., Campbell, C. L., Cernusca, A., Cescatti, A., Clifton-Brown, J., Dirks, B. O.
954 M., Dore, S., Eugster, W., Fuhrer, J., Gimeno, C., Gruenwald, T., Haszpra, L., Hensen, A.,
955 Ibrom, A., Jacobs, A. F. G., Jones, M. B., Lanigan, G., Laurila, T., Lohila, A., G. Manca,
956 Marcolla, B., Nagy, Z., Pilegaard, K., Pinter, K., Pio, C., Raschi, A., Rogiers, N., Sanz, M. J.,
957 Stefani, P., Sutton, M., Tuba, Z., Valentini, R., Williams, M. L., and Wohlfahrt, G.:
958 Partitioning European grassland net ecosystem CO₂ exchange into gross primary productivity
959 and ecosystem respiration using light response function analysis, *Agriculture, Ecosystems &
960 Environment*, 121, 93-120, 10.1016/j.agee.2006.12.008, 2007.
- 961 Gocic, M., and Trajkovic, S.: Analysis of trends in reference evapotranspiration data in a
962 humid climate, *Hydrological Sciences Journal*, 59, 165-180, 10.1080/02626667.2013.798659,
963 2013.
- 964 Gold, C. M.: Surface interpolation, spatial adjacency and GIS, in: *Three Dimensional
965 Applications in Geographical Information Systems*, edited by: Raper, J., Taylor and Francis,
966 London, 1989.
- 967 Green, D. A.: A colour scheme for the display of astronomical intensity images, *Bulletin of
968 the Astronomical Society of India*, 39, 2011.
- 969 Haddeland, I., Clark, D. B., Franssen, W., Ludwig, F., Voß, F., Arnell, N. W., Bertrand, N.,
970 Best, M., Folwell, S., Gerten, D., Gomes, S., Gosling, S. N., Hagemann, S., Hanasaki, N.,
971 Harding, R., Heinke, J., Kabat, P., Koirala, S., Oki, T., Polcher, J., Stacke, T., Viterbo, P.,
972 Weedon, G. P., and Yeh, P.: Multimodel Estimate of the Global Terrestrial Water Balance:
973 Setup and First Results, *Journal of Hydrometeorology*, 12, 869-884, 10.1175/2011jhm1324.1,
974 2011.
- 975 Hannaford, J., and Buys, G.: Trends in seasonal river flow regimes in the UK, *Journal of
976 Hydrology*, 475, 158-174, doi:10.1016/j.jhydrol.2012.09.044, 2012.
- 977 Hannaford, J.: Climate-driven changes in UK river flows: A review of the evidence, *Progress
978 in Physical Geography*, 39, 29-48, doi:10.1177/0309133314536755, 2015.

979 Harris, I., Jones, P. D., Osborn, T. J., and Lister, D. H.: Updated high-resolution grids of
980 monthly climatic observations - the CRU TS3.10 Dataset, *International Journal of*
981 *Climatology*, 34, 623-642, doi:10.1002/Joc.3711, 2014.

982 Hartmann, D. L., Klein Tank, A. M. G., Rusticucci, M., Alexander, L. V., Brönnimann, S.,
983 Charabi, Y., Dentener, F. J., Dlugokencky, E. J., Easterling, D. R., Kaplan, A., Soden, B. J.,
984 Thorne, P. W., Wild, M., and Zhai, P. M.: Observations: Atmosphere and Surface, in: *Climate*
985 *Change 2013: The Physical Science Basis. Contribution of Working Group I to the Fifth*
986 *Assessment Report of the Intergovernmental Panel on Climate Change*, edited by: Stocker, T.
987 F., Qin, D., Plattner, G.-K., Tignor, M., Allen, S. K., Boschung, J., Nauels, A., Xia, Y., Bex,
988 V., and Midgley, P. M., Cambridge University Press, Cambridge, United Kingdom and New
989 York, NY, USA, 159–254, 2013.

990 Haslinger, K., and Bartsch, A.: Creating long-term gridded fields of reference
991 evapotranspiration in Alpine terrain based on a recalibrated Hargreaves method, *Hydrology*
992 *and Earth System Sciences*, 20, 1211-1223, 10.5194/hess-20-1211-2016, 2016.

993 Heinemeyer, A., Wilkinson, M., Vargas, R., Subke, J. A., Casella, E., Morison, J. I. L., and
994 Ineson, P.: Exploring the "overflow tap" theory: linking forest soil CO₂ fluxes
995 and individual mycorrhizosphere components to photosynthesis, *Biogeosciences*, 9, 79-95,
996 10.5194/bg-9-79-2012, 2012.

997 Helmes, L., and Jaenicke, R.: Atmospheric turbidity determined from sunshine records,
998 *Journal of Aerosol Science*, 17, 261-263, doi:10.1016/0021-8502(86)90080-7, 1986.

999 Hickling, R., Roy, D. B., Hill, J. K., Fox, R., and Thomas, C. D.: The distributions of a wide
1000 range of taxonomic groups are expanding polewards, *Global Change Biology*, 12, 450-455,
1001 doi:10.1111/j.1365-2486.2006.01116.x, 2006.

1002 Horn, B. K. P.: Hill Shading and the Reflectance Map, *P IEEE*, 69, 14-47,
1003 doi:10.1109/Proc.1981.11918, 1981.

1004 Hosseinzadeh Talae, P., Shifteh Some'e, B., and Sobhan Ardakani, S.: Time trend and
1005 change point of reference evapotranspiration over Iran, *Theoretical and Applied Climatology*,
1006 116, 639-647, 10.1007/s00704-013-0978-x, 2013.

1007 Hough, M. N., and Jones, R. J. A.: The United Kingdom Meteorological Office rainfall and
1008 evaporation calculation system: MORECS version 2.0-an overview, *Hydrology and Earth*
1009 *System Sciences*, 1, 227-239, doi:10.5194/hess-1-227-1997, 1997.

1010 IPCC: *Climate Change 2013: The Physical Science Basis. Contribution of Working Group I*
1011 *to the Fifth Assessment Report of the Intergovernmental Panel on Climate Change*,
1012 Cambridge University Press, Cambridge, United Kingdom and New York, NY, USA, 1535
1013 pp., 2013.

1014 IPCC: *Climate Change 2014: Impacts, Adaptation, and Vulnerability. Part A: Global and*
1015 *Sectoral Aspects. Contribution of Working Group II to the Fifth Assessment Report of the*
1016 *Intergovernmental Panel on Climate Change* [Field, C.B., V.R. Barros, D.J. Dokken, K.J.
1017 Mach, M.D. Mastrandrea, T.E. Bilir, M. Chatterjee, K.L. Ebi, Y.O. Estrada, R.C. Genova, B.
1018 Girma, E.S. Kissel, A.N. Levy, S. MacCracken, P.R. Mastrandrea, and L.L. White (eds.)],
1019 Cambridge University Press, Cambridge, United Kingdom and New York, NY, USA, 1132
1020 pp., 2014a.

1021 IPCC: *Climate Change 2014: Impacts, Adaptation, and Vulnerability. Part B: Regional*
1022 *Aspects. Contribution of Working Group II to the Fifth Assessment Report of the*

- 1023 Intergovernmental Panel on Climate Change [Barros, V.R., C.B. Field, D.J. Dokken, M.D.
1024 Mastrandrea, K.J. Mach, T.E. Bilir, M. Chatterjee, K.L. Ebi, Y.O. Estrada, R.C. Genova, B.
1025 Girma, E.S. Kissel, A.N. Levy, S. MacCracken, P.R. Mastrandrea, and L.L. White (eds.)],
1026 Cambridge University Press, Cambridge, United Kingdom and New York, NY, USA, 688
1027 pp., 2014b.
- 1028 Iqbal, M.: An introduction to solar radiation, Academic Press, London, 1983.
- 1029 Ishibashi, M., and Terashima, I.: Effects of continuous leaf wetness on photosynthesis:
1030 adverse aspects of rainfall, *Plant, Cell & Environment*, 18, 431-438, 10.1111/j.1365-
1031 3040.1995.tb00377.x, 1995.
- 1032 Jenkins, G. J., Perry, M. C., and Prior, M. J.: The climate of the United Kingdom and recent
1033 trends, Met Office Hadley Centre, Exeter, UK, 2008.
- 1034 Jhajharia, D., Dinpashoh, Y., Kahya, E., Singh, V. P., and Fakheri-Fard, A.: Trends in
1035 reference evapotranspiration in the humid region of northeast India, *Hydrological Processes*,
1036 26, 421-435, 10.1002/hyp.8140, 2012.
- 1037 Jones, P. D., Lister, D. H., Osborn, T. J., Harpham, C., Salmon, M., and Morice, C. P.:
1038 Hemispheric and large-scale land-surface air temperature variations: An extensive revision
1039 and an update to 2010, *Journal of Geophysical Research: Atmospheres*, 117, n/a-n/a,
1040 doi:10.1029/2011JD017139, 2012.
- 1041 Jones, P. D., and Harris, I.: CRU TS3.21: Climatic Research Unit (CRU) Time-Series (TS)
1042 Version 3.21 of High Resolution Gridded Data of Month-by-month Variation in Climate (Jan.
1043 1901- Dec. 2012). University of East Anglia Climatic Research Unit,
1044 doi:10.5285/D0E1585D-3417-485F-87AE-4FCECF10A992, 2013.
- 1045 Kay, A. L., Bell, V. A., Blyth, E. M., Crooks, S. M., Davies, H. N., and Reynard, N. S.: A
1046 hydrological perspective on evaporation: historical trends and future projections in Britain,
1047 *Journal of Water and Climate Change*, 4, 193, doi:10.2166/wcc.2013.014, 2013.
- 1048 Kay, A. L., Rudd, A. C., Davies, H. N., Kendon, E. J., and Jones, R. G.: Use of very high
1049 resolution climate model data for hydrological modelling: baseline performance and future
1050 flood changes, *Climatic Change*, doi:10.1007/s10584-015-1455-6, 2015.
- 1051 Keller, V. D. J., Tanguy, M., Prodocimi, I., Terry, J. A., Hitt, O., Cole, S. J., Fry, M., Morris,
1052 D. G., and Dixon, H.: CEH-GEAR: 1 km resolution daily and monthly areal rainfall estimates
1053 for the UK for hydrological and other applications, *Earth Syst. Sci. Data*, 7, 143-155,
1054 doi:10.5194/essd-7-143-2015, 2015.
- 1055 Kimball, B. A., Idso, S. B., and Aase, J. K.: A Model of Thermal-Radiation from Partly
1056 Cloudy and Overcast Skies, *Water Resources Research*, 18, 931-936,
1057 doi:10.1029/Wr018i004p00931, 1982.
- 1058 Kruijt, B., Witte, J.-P. M., Jacobs, C. M. J., and Kroon, T.: Effects of rising atmospheric CO₂
1059 on evapotranspiration and soil moisture: A practical approach for the Netherlands, *Journal of*
1060 *Hydrology*, 349, 257-267, doi:10.1016/j.jhydrol.2007.10.052, 2008.
- 1061 Kume, T., Kuraji, K., Yoshifuji, N., Morooka, T., Sawano, S., Chong, L., and Suzuki, M.:
1062 Estimation of canopy drying time after rainfall using sap flow measurements in an emergent
1063 tree in a lowland mixed-dipterocarp forest in Sarawak, Malaysia, *Hydrological Processes*, 20,
1064 565-578, 10.1002/hyp.5924, 2006.
- 1065 Lange, O. L., Lösch, R., Schulze, E.-D., and Kappen, L.: Responses of stomata to changes in
1066 humidity, *Planta*, 100, 76-86, 10.1007/bf00386887, 1971.

- 1067 Li, B., Chen, F., and Guo, H.: Regional complexity in trends of potential evapotranspiration
1068 and its driving factors in the Upper Mekong River Basin, *Quaternary International*, 380-381,
1069 83-94, 10.1016/j.quaint.2014.12.052, 2015.
- 1070 Li, Y., and Zhou, M.: Trends in Dryness Index Based on Potential Evapotranspiration and
1071 Precipitation over 1961–2099 in Xinjiang, China, *Advances in Meteorology*, 2014, 1-15,
1072 10.1155/2014/548230, 2014.
- 1073 Liley, J. B.: New Zealand dimming and brightening, *Journal of Geophysical Research*, 114,
1074 doi:10.1029/2008jd011401, 2009.
- 1075 Lu, X., Bai, H., and Mu, X.: Explaining the evaporation paradox in Jiangxi Province of
1076 China: Spatial distribution and temporal trends in potential evapotranspiration of Jiangxi
1077 Province from 1961 to 2013, *International Soil and Water Conservation Research*, 4, 45-51,
1078 10.1016/j.iswcr.2016.02.004, 2016.
- 1079 Marsh, T., and Dixon, H.: The UK water balance – how much has it changed in a warming
1080 world?, 01-05, doi:10.7558/bhs.2012.ns32, 2012.
- 1081 Marthews, T. R., Malhi, Y., and Iwata, H.: Calculating downward longwave radiation under
1082 clear and cloudy conditions over a tropical lowland forest site: an evaluation of model
1083 schemes for hourly data, *Theoretical and Applied Climatology*, 107, 461-477,
1084 10.1007/s00704-011-0486-9, 2011.
- 1085 Matsoukas, C., Benas, N., Hatzianastassiou, N., Pavlakis, K. G., Kanakidou, M., and
1086 Vardavas, I.: Potential evaporation trends over land between 1983–2008: driven by radiative
1087 fluxes or vapour-pressure deficit?, *Atmospheric Chemistry and Physics*, 11, 7601-7616,
1088 doi:10.5194/acp-11-7601-2011, 2011.
- 1089 McVicar, T. R., Van Niel, T. G., Li, L. T., Roderick, M. L., Rayner, D. P., Ricciardulli, L.,
1090 and Donohue, R. J.: Wind speed climatology and trends for Australia, 1975–2006: Capturing
1091 the stilling phenomenon and comparison with near-surface reanalysis output, *Geophysical
1092 Research Letters*, 35, n/a-n/a, 10.1029/2008GL035627, 2008.
- 1093 McVicar, T. R., Roderick, M. L., Donohue, R. J., Li, L. T., Van Niel, T. G., Thomas, A.,
1094 Grieser, J., Jhajharia, D., Himri, Y., Mahowald, N. M., Mescherskaya, A. V., Kruger, A. C.,
1095 Rehman, S., and Dinpashoh, Y.: Global review and synthesis of trends in observed terrestrial
1096 near-surface wind speeds: Implications for evaporation, *Journal of Hydrology*, 416, 182-205,
1097 doi:10.1016/j.jhydrol.2011.10.024, 2012.
- 1098 Monteith, J. L.: *Evaporation and environment*, in: 19th Symposia of the Society for
1099 Experimental Biology, University Press, Cambridge, 1965.
- 1100 Moors, E.: *Water Use of Forests in the Netherlands*, PhD, Vrije Universiteit, Amsterdam, the
1101 Netherlands, 2012.
- 1102 Morris, D. G., and Flavin, R. W.: A digital terrain model for hydrology., *Proceedings of the
1103 4th International Symposium on Spatial Data Handling*, 1, 250-262, 1990.
- 1104 Morton, D., Rowland, C., Wood, C., Meek, L., Marston, C., Smith, G., Wadsworth, R., and
1105 Simpson, I. C.: *Final Report for LCM2007 - the new UK land cover map*, NERC/Centre for
1106 Ecology & Hydrology 11/07 (CEH Project Number: C03259), 2011.
- 1107 Muneer, T., and Munawwar, S.: Potential for improvement in estimation of solar diffuse
1108 irradiance, *Energ Convers Manage*, 47, 68-86, doi:10.1016/j.enconman.2005.03.015, 2006.

- 1109 Murphy, J. M., Sexton, D. M. H., Jenkins, G. J., Boorman, P. M., Booth, B. B. B., Brown, C.
1110 C., Clark, R. T., Collins, M., Harris, G. R., Kendon, E. J., Betts, R. A., Brown, S. J., Howard,
1111 T. P., Humphrey, K. A., McCarthy, M. P., McDonald, R. E., Stephens, A., Wallace, C.,
1112 Warren, R., Wilby, R., and Wood, R. A.: UK Climate Projections Science Report: Climate
1113 change projections, Met Office Hadley Centre, Exeter, 2009.
- 1114 Newton, K., and Burch, S. F.: Estimation of the UK wind energy resource using computer
1115 modelling techniques and map data, Energy Technology Support Unit, 50, 1985.
- 1116 Norton, L. R., Maskell, L. C., Smart, S. S., Dunbar, M. J., Emmett, B. A., Carey, P. D.,
1117 Williams, P., Crowe, A., Chandler, K., Scott, W. A., and Wood, C. M.: Measuring stock and
1118 change in the GB countryside for policy--key findings and developments from the
1119 Countryside Survey 2007 field survey, *Journal of environmental management*, 113, 117-127,
1120 doi:10.1016/j.jenvman.2012.07.030, 2012.
- 1121 Oldekop, E.: Evaporation from the surface of river basins, in: *Collection of the Works of*
1122 *Students of the Meteorological Observatory, University of Tartu-Jurjew-Dorpat, Tartu,*
1123 *Estonia*, 209, 1911.
- 1124 Palmer, W. C.: *Meteorological Drought. Res. Paper No.45, Dept. of Commerce, Washington,*
1125 *D.C., 1965.*
- 1126 Paltineanu, C., Chitu, E., and Mateescu, E.: New trends for reference evapotranspiration and
1127 climatic water deficit, *International Agrophysics*, 26, 10.2478/v10247-012-0023-9, 2012.
- 1128 Parker, D., and Horton, B.: Uncertainties in central England temperature 1878-2003 and some
1129 improvements to the maximum and minimum series, *International Journal of Climatology*, 25,
1130 1173-1188, doi:10.1002/joc.1190, 2005.
- 1131 Penman, H. L.: Natural Evaporation from Open Water, Bare Soil and Grass, *Proceedings of*
1132 *the Royal Society of London. Series A. Mathematical and Physical Sciences*, 193, 120-145,
1133 10.1098/rspa.1948.0037, 1948.
- 1134 Pocock, M. J., Roy, H. E., Preston, C. D., and Roy, D. B.: The Biological Records Centre in
1135 the United Kingdom: a pioneer of citizen science., *Biological Journal of the Linnean Society*,
1136 doi:10.1111/bij.12548, 2015.
- 1137 Prata, A. J.: A new long-wave formula for estimating downward clear-sky radiation at the
1138 surface, *Quarterly Journal of the Royal Meteorological Society*, 122, 1127-1151,
1139 doi:10.1002/qj.49712253306, 1996.
- 1140 Prescott, J. A.: Evaporation from a water surface in relation to solar radiation, *Transaction of*
1141 *the Royal Society of South Australia*, 64, 114-125, 1940.
- 1142 Prudhomme, C., Giuntoli, I., Robinson, E. L., Clark, D. B., Arnell, N. W., Dankers, R.,
1143 Fekete, B. M., Franssen, W., Gerten, D., Gosling, S. N., Hagemann, S., Hannah, D. M., Kim,
1144 H., Masaki, Y., Satoh, Y., Stacke, T., Wada, Y., and Wisser, D.: Hydrological droughts in the
1145 21st century, hotspots and uncertainties from a global multimodel ensemble experiment,
1146 *Proceedings of the National Academy of Sciences*, 111, 3262-3267,
1147 doi:10.1073/pnas.1222473110, 2014.
- 1148 Pryor, S. C., Barthelmie, R. J., Young, D. T., Takle, E. S., Arritt, R. W., Flory, D., Gutowski,
1149 W. J., Nunes, A., and Roads, J.: Wind speed trends over the contiguous United States, *Journal*
1150 *of Geophysical Research: Atmospheres*, 114, n/a-n/a, 10.1029/2008JD011416, 2009.
- 1151 Reynolds, B., Chamberlain, P. M., Poskitt, J., Woods, C., Scott, W. A., Rowe, E. C.,
1152 Robinson, D. A., Frogbrook, Z. L., Keith, A. M., Henrys, P. A., Black, H. I. J., and Emmett,

- 1153 B. A.: Countryside Survey: National “Soil Change” 1978–2007 for Topsoils in Great
1154 Britain—Acidity, Carbon, and Total Nitrogen Status, *Vadose Zone Journal*, 12, 0,
1155 doi:10.2136/vzj2012.0114, 2013.
- 1156 Richards, J. M.: A simple expression for the saturation vapour pressure of water in the range
1157 –50 to 140°C, *Journal of Physics D: Applied Physics*, 4, L15, 1971.
- 1158 Robinson, E. L., Blyth, E., Clark, D. B., Finch, J., and Rudd, A. C.: Climate hydrology and
1159 ecology research support system potential evapotranspiration dataset for Great Britain (1961-
1160 2012) [CHESS-PE], NERC-Environmental Information Data Centre, 2015a.
- 1161 Robinson, E. L., Blyth, E., Clark, D. B., Finch, J., and Rudd, A. C.: Climate hydrology and
1162 ecology research support system meteorology dataset for Great Britain (1961-2012) [CHESS-
1163 met], NERC-Environmental Information Data Centre, 2015b.
- 1164 Rodda, J. C., and Marsh, T. J.: The 1975-76 Drought - a contemporary and retrospective
1165 review, Wallingford, UK, 2011.
- 1166 Roderick, M. L., Rotstayn, L. D., Farquhar, G. D., and Hobbins, M. T.: On the attribution of
1167 changing pan evaporation, *Geophysical Research Letters*, 34, 10.1029/2007gl031166, 2007.
- 1168 Rotstayn, L. D., Roderick, M. L., and Farquhar, G. D.: A simple pan-evaporation model for
1169 analysis of climate simulations: Evaluation over Australia, *Geophysical Research Letters*, 33,
1170 10.1029/2006gl027114, 2006.
- 1171 Rudd, A. C., and Kay, A. L.: Use of very high resolution climate model data for hydrological
1172 modelling: estimation of potential evaporation, *Hydrology Research*, doi:
1173 10.2166/nh.2015.028, 2015.
- 1174 Rutter, A. J., Kershaw, K. A., Robins, P. C., and Morton, A. J.: A predictive model of rainfall
1175 interception in forests, 1. Derivation of the model from observations in a plantation of
1176 Corsican pine, *Agricultural Meteorology*, 9, 367-384, doi:10.1016/0002-1571(71)90034-3,
1177 1971.
- 1178 Sanchez-Lorenzo, A., Calbó, J., and Martin-Vide, J.: Spatial and Temporal Trends in
1179 Sunshine Duration over Western Europe (1938–2004), *Journal of Climate*, 21, 6089-6098,
1180 doi:10.1175/2008jcli2442.1, 2008.
- 1181 Sanchez-Lorenzo, A., Calbó, J., Brunetti, M., and Deser, C.: Dimming/brightening over the
1182 Iberian Peninsula: Trends in sunshine duration and cloud cover and their relations with
1183 atmospheric circulation, *Journal of Geophysical Research*, 114, doi:10.1029/2008jd011394,
1184 2009.
- 1185 Sanchez-Lorenzo, A., and Wild, M.: Decadal variations in estimated surface solar radiation
1186 over Switzerland since the late 19th century, *Atmospheric Chemistry and Physics*, 12, 8635-
1187 8644, doi:10.5194/acp-12-8635-2012, 2012.
- 1188 Sanchez-Romero, A., Sanchez-Lorenzo, A., Calbó, J., González, J. A., and Azorin-Molina,
1189 C.: The signal of aerosol-induced changes in sunshine duration records: A review of the
1190 evidence, *Journal of Geophysical Research: Atmospheres*, 119, 4657-4673,
1191 doi:10.1002/2013JD021393, 2014.
- 1192 Scheff, J., and Frierson, D. M. W.: Scaling Potential Evapotranspiration with Greenhouse
1193 Warming, *Journal of Climate*, 27, 1539-1558, doi:10.1175/JCLI-D-13-00233.1, 2014.

- 1194 Schymanski, S. J., and Or, D.: Wind effects on leaf transpiration challenge the concept of
1195 "potential evaporation", *Proceedings of the International Association of Hydrological*
1196 *Sciences*, 371, 99-107, 10.5194/piahs-371-99-2015, 2015.
- 1197 Shan, N., Shi, Z., Yang, X., Zhang, X., Guo, H., Zhang, B., and Zhang, Z.: Trends in potential
1198 evapotranspiration from 1960 to 2013 for a desertification-prone region of China,
1199 *International Journal of Climatology*, n/a-n/a, 10.1002/joc.4566, 2015.
- 1200 Sheffield, J., Goteti, G., and Wood, E. F.: Development of a 50-Year High-Resolution Global
1201 Dataset of Meteorological Forcings for Land Surface Modeling, *Journal of Climate*, 19, 3088-
1202 3111, doi:10.1175/JCLI3790.1, 2006.
- 1203 Shuttleworth, W. J.: *Terrestrial Hydrometeorology*, John Wiley & Sons, Ltd, 2012.
- 1204 Song, Z. W. Z., H. L. ; Snyder, R. L. ;Anderson, F. E. ;Chen, F. : Distribution and Trends in
1205 Reference Evapotranspiration in the North China Plain, *Journal of Irrigation and Drainage*
1206 *Engineering*, 136, 240-247, doi:10.1061/(ASCE)IR.1943-4774.0000175, 2010.
- 1207 Soussana, J. F., Allard, V., Pilegaard, K., Ambus, P., Amman, C., Campbell, C., Ceschia, E.,
1208 Clifton-Brown, J., Czobel, S., Domingues, R., Flechard, C., Fuhrer, J., Hensen, A., Horvath,
1209 L., Jones, M., Kasper, G., Martin, C., Nagy, Z., Neftel, A., Raschi, A., Baronti, S., Rees, R.
1210 M., Skiba, U., Stefani, P., Manca, G., Sutton, M., Tuba, Z., and Valentini, R.: Full accounting
1211 of the greenhouse gas (CO₂, N₂O, CH₄) budget of nine European grassland sites,
1212 *Agriculture, Ecosystems & Environment*, 121, 121-134, 10.1016/j.agee.2006.12.022, 2007.
- 1213 Stanhill, G., and Cohen, S.: Solar Radiation Changes in the United States during the
1214 Twentieth Century: Evidence from Sunshine Duration Measurements, *Journal of Climate*, 18,
1215 1503-1512, doi:10.1175/JCLI3354.1, 2005.
- 1216 Stanhill, G., and Möller, M.: Evaporative climate change in the British Isles, *International*
1217 *Journal of Climatology*, 28, 1127-1137, doi:10.1002/joc.1619, 2008.
- 1218 Stewart, J. B.: On the use of the Penman-Monteith equation for determining areal
1219 evapotranspiration, in: *Estimation of Areal Evapotranspiration (Proceedings of a workshop*
1220 *held at Vancouver, B.C., Canada, August 1987)*. edited by: Black, T. A. S., D. L.; Novak, M.
1221 D.; Price, D. T., IAHS, Wallingford, Oxfordshire, UK, 1989.
- 1222 Sutton, R. T., and Dong, B.: Atlantic Ocean influence on a shift in European climate in the
1223 1990s, *Nature Geosci*, 5, 788-792, doi:10.1038/ngeo1595, 2012.
- 1224 Tabari, H., Nikbakht, J., and Hosseinzadeh Talae, P.: Identification of Trend in Reference
1225 Evapotranspiration Series with Serial Dependence in Iran, *Water Resources Management*, 26,
1226 2219-2232, 10.1007/s11269-012-0011-7, 2012.
- 1227 Tanguy, M., Dixon, H., Prosdocimi, I., Morris, D. G., and Keller, V. D. J.: Gridded estimates
1228 of daily and monthly areal rainfall for the United Kingdom (1890-2012) [CEH-GEAR],
1229 NERC Environmental Information Data Centre, doi:10.5285/5dc179dc-f692-49ba-9326-
1230 a6893a503f6e, 2014.
- 1231 Thackeray, S. J., Sparks, T. H., Frederiksen, M., Burthe, S., Bacon, P. J., Bell, J. R., Botham,
1232 M. S., Brereton, T. M., Bright, P. W., Carvalho, L., Clutton-Brock, T., Dawson, A., Edwards,
1233 M., Elliott, J. M., Harrington, R., Johns, D., Jones, I. D., Jones, J. T., Leech, D. I., Roy, D. B.,
1234 Scott, W. A., Smith, M., Smithers, R. J., Winfield, I. J., and Wanless, S.: Trophic level
1235 asynchrony in rates of phenological change for marine, freshwater and terrestrial
1236 environments, *Global Change Biology*, 16, 3304-3313, doi:10.1111/j.1365-
1237 2486.2010.02165.x, 2010.

- 1238 Thompson, N., Barrie, I. A., and Ayles, M.: The Meteorological Office rainfall and
1239 evaporation calculation system: MORECS, Meteorological Office, Bracknell, 1981.
- 1240 Vautard, R., Cattiaux, J., Yiou, P., Thepaut, J. N., and Ciais, P.: Northern Hemisphere
1241 atmospheric stilling partly attributed to an increase in surface roughness, *Nature Geoscience*,
1242 3, 756-761, doi:10.1038/Ngeo979, 2010.
- 1243 Vicente-Serrano, S. M., Azorin-Molina, C., Sanchez-Lorenzo, A., Revuelto, J., López-
1244 Moreno, J. I., González-Hidalgo, J. C., Moran-Tejeda, E., and Espejo, F.: Reference
1245 evapotranspiration variability and trends in Spain, 1961–2011, *Global and Planetary Change*,
1246 121, 26-40, 10.1016/j.gloplacha.2014.06.005, 2014.
- 1247 Vicente-Serrano, S. M., Azorin-Molina, C., Sanchez-Lorenzo, A., El Kenawy, A., Martín-
1248 Hernández, N., Peña-Gallardo, M., Beguería, S., and Tomas-Burguera, M.: Recent changes
1249 and drivers of the atmospheric evaporative demand in the Canary Islands, *Hydrology and
1250 Earth System Sciences Discussions*, 1-35, 10.5194/hess-2016-15, 2016.
- 1251 Vincent, L. A., Zhang, X., Brown, R. D., Feng, Y., Mekis, E., Milewska, E. J., Wan, H., and
1252 Wang, X. L.: Observed Trends in Canada's Climate and Influence of Low-Frequency
1253 Variability Modes, *Journal of Climate*, 28, 4545-4560, 10.1175/jcli-d-14-00697.1, 2015.
- 1254 von Storch, H., and Zwiers, F. W.: *Statistical analysis in climate research*, Cambridge
1255 University Press, Cambridge ; New York, x, 484 p. pp., 1999.
- 1256 Wang, K., and Liang, S.: Global atmospheric downward longwave radiation over land surface
1257 under all-sky conditions from 1973 to 2008, *Journal of Geophysical Research*, 114,
1258 doi:10.1029/2009jd011800, 2009.
- 1259 Ward, R. C., and Robinson, M.: *Principles of Hydrology*, McGraw Hill, 2000.
- 1260 Watts, G., Battarbee, R. W., Bloomfield, J. P., Crossman, J., Daccache, A., Durance, I.,
1261 Elliott, J. A., Garner, G., Hannaford, J., Hannah, D. M., Hess, T., Jackson, C. R., Kay, A. L.,
1262 Kernan, M., Knox, J., Mackay, J., Monteith, D. T., Ormerod, S. J., Rance, J., Stuart, M. E.,
1263 Wade, A. J., Wade, S. D., Weatherhead, K., Whitehead, P. G., and Wilby, R. L.: Climate
1264 change and water in the UK - past changes and future prospects, *Progress in Physical
1265 Geography*, 39, 6-28, doi:10.1177/0309133314542957, 2015.
- 1266 Weedon, G. P., Gomes, S., Viterbo, P., Shuttleworth, W. J., Blyth, E., Osterle, H., Adam, J.
1267 C., Bellouin, N., Boucher, O., and Best, M.: Creation of the WATCH Forcing Data and Its
1268 Use to Assess Global and Regional Reference Crop Evaporation over Land during the
1269 Twentieth Century, *Journal of Hydrometeorology*, 12, 823-848, doi:10.1175/2011jhm1369.1,
1270 2011.
- 1271 Weedon, G. P., Balsamo, G., Bellouin, N., Gomes, S., Best, M. J., and Viterbo, P.: The
1272 WFDEI meteorological forcing data set: WATCH Forcing Data methodology applied to
1273 ERA-Interim reanalysis data, *Water Resources Research*, 50, 7505-7514,
1274 doi:10.1002/2014WR015638, 2014.
- 1275 Wild, M.: Global dimming and brightening: A review, *Journal of Geophysical Research*, 114,
1276 doi:10.1029/2008jd011470, 2009.
- 1277 Wilkinson, M., Eaton, E. L., Broadmeadow, M. S. J., and Morison, J. I. L.: Inter-annual
1278 variation of carbon uptake by a plantation oak woodland in south-eastern England,
1279 *Biogeosciences*, 9, 5373-5389, 10.5194/bg-9-5373-2012, 2012.
- 1280 Willett, K. M., Dunn, R. J. H., Thorne, P. W., Bell, S., de Podesta, M., Parker, D. E., Jones, P.
1281 D., and Williams Jr, C. N.: HadISDH land surface multi-variable humidity and temperature

1282 record for climate monitoring, *Climate of the Past*, 10, 1983-2006, 10.5194/cp-10-1983-2014,
1283 2014.

1284 WMO: Manual on the Global Observing System, Secretariat of the World Meteorological
1285 Organization, Geneva, Switzerland, 2013.

1286 Wood, C. M., Smart, S. M., and Bunce, R. G. H.: Woodland survey of Great Britain 1971–
1287 2001, *Earth System Science Data Discussions*, 8, 259-277, doi:10.5194/essdd-8-259-2015,
1288 2015.

1289 Yin, Y., Wu, S., Chen, G., and Dai, E.: Attribution analyses of potential evapotranspiration
1290 changes in China since the 1960s, *Theoretical and Applied Climatology*, 101, 19-28,
1291 10.1007/s00704-009-0197-7, 2009.

1292 Zhang, K.-x., Pan, S.-m., Zhang, W., Xu, Y.-h., Cao, L.-g., Hao, Y.-p., and Wang, Y.:
1293 Influence of climate change on reference evapotranspiration and aridity index and their
1294 temporal-spatial variations in the Yellow River Basin, China, from 1961 to 2012, *Quaternary
1295 International*, 380-381, 75-82, 10.1016/j.quaint.2014.12.037, 2015.

1296 Zhao, J., Xu, Z.-x., Zuo, D.-p., and Wang, X.-m.: Temporal variations of reference
1297 evapotranspiration and its sensitivity to meteorological factors in Heihe River Basin, China,
1298 *Water Science and Engineering*, 8, 1-8, 10.1016/j.wse.2015.01.004, 2015.

1299 Zwiers, F. W., and von Storch, H.: Taking Serial-Correlation into Account in Tests of the
1300 Mean, *Journal of Climate*, 8, 336-351, doi:10.1175/1520-
1301 0442(1995)008<0336:Tsciai>2.0.Co;2, 1995.

1302

1303

1304 Table 1. Description of input meteorological variables

| Variable (units) | Source data | Ancillary files | Assumptions | Height |
|--|--|--|---|--------|
| Air temperature (K) | MORECS air temperature | IHDTM elevation | Lapsed to IHDTM elevation | 1.2 m |
| Specific humidity (kg kg ⁻¹) | MORECS vapour pressure | IHDTM elevation | Lapsed to IHDTM elevation Constant air pressure = 1 kPa | 1.2 m |
| Downward LW radiation (W m ⁻²) | MORECS air temperature, vapour pressure, sunshine hours | IHDTM elevation | Constant cloud base height | 1.2 m |
| Downward SW radiation (W m ⁻²) | MORECS sunshine hours | IHDTM elevation Spatially-varying aerosol correction | No time-varying aerosol correction | 1.2 m |
| Wind speed (m s ⁻¹) | MORECS wind speed | ETSU average wind speeds | Wind speed correction is constant | 10 m |
| Precipitation (kg m ⁻² s ⁻¹) | CEH-GEAR precipitation | - | No transformations performed | n/a |
| Daily temperature range (K) | CRU TS 3.21 daily temperature range | - | No spatial interpolation from 0.5° resolution. No temporal interpolation (constant values for each month) | 1.2 m |

| | | | | |
|---------------------------|------------------|-----------------|---|-----|
| Surface air pressure (Pa) | WFD air pressure | IHDTM elevation | Mean-monthly values from WFD used (each year has same values). Lapsed to IHDTM elevation. No temporal interpolation (constant values for each month). | n/a |
|---------------------------|------------------|-----------------|---|-----|

1305
1306

1307 Table 2: Rate of change of annual means of meteorological and potential evapotranspiration
 1308 variables in Great Britain. Bold indicates trends that are significant at the 5% level. The
 1309 ranges are given by the 95% CI.

| Variable | Rate of change \pm 95% CI | | | | |
|--|-------------------------------------|-------------------------------------|-------------------------------------|-------------------------------------|-------------------------------------|
| | Great Britain | England | Scotland | Wales | English lowlands |
| Air temperature (K dec ⁻¹) | 0.21 \pm 0.15 | 0.23 \pm 0.14 | 0.17 \pm 0.12 | 0.21 \pm 0.15 | 0.25 \pm 0.17 |
| Specific humidity (g kg ⁻¹ dec ⁻¹) | 0.049 \pm 0.037 | 0.054 \pm 0.04 | 0.040 \pm 0.036 | 0.055 \pm 0.037 | 0.053 \pm 0.044 |
| Downward SW radiation (W m ⁻² dec ⁻¹) | 1.0 \pm 0.8 | 1.3 \pm 1.0 | 0.5 \pm 0.6 | 1.1 \pm 0.9 | 1.5 \pm 1.0 |
| Downward LW radiation (W m ⁻² dec ⁻¹) | 0.50 \pm 0.48 | 0.45 \pm 0.48 | 0.58 \pm 0.48 | 0.50 \pm 0.55 | 0.42 \pm 0.48 |
| Wind speed (m s ⁻¹ dec ⁻¹) | -0.18 \pm 0.09 | -0.16 \pm 0.09 | -0.20 \pm 0.10 | -0.25 \pm 0.16 | -0.13 \pm 0.07 |
| Precipitation (mm d ⁻¹ dec ⁻¹) | 0.08 \pm 0.06 | 0.04 \pm 0.06 | 0.14 \pm 0.09 | 0.08 \pm 0.09 | 0.03 \pm 0.05 |
| Daily temperature range (K dec ⁻¹) | -0.06 \pm 0.06 | -0.03 \pm 0.06 | -0.13 \pm 0.08 | 0.00 \pm 0.06 | -0.04 \pm 0.07 |
| Relative humidity (% dec ⁻¹) | -0.39 \pm 0.44 | -0.43 \pm 0.46 | -0.33 \pm 0.33 | -0.36 \pm 0.4 | -0.50 \pm 0.53 |
| PET (mm d ⁻¹ dec ⁻¹) | 0.021 \pm 0.021 | 0.025 \pm 0.024 | 0.015 \pm 0.015 | 0.017 \pm 0.021 | 0.03 \pm 0.026 |
| Radiative component of PET (mm d ⁻¹ dec ⁻¹) | 0.016 \pm 0.010 | 0.018 \pm 0.011 | 0.013 \pm 0.008 | 0.020 \pm 0.013 | 0.018 \pm 0.011 |
| Aerodynamic component of PET (mm d ⁻¹ dec ⁻¹) | 0.007 \pm 0.011 | 0.009 \pm 0.013 | 0.004 \pm 0.009 | 0.001 \pm 0.013 | 0.015 \pm 0.015 |
| PETI (mm d ⁻¹ dec ⁻¹) | 0.019 \pm 0.020 | 0.023 \pm 0.023 | 0.014 \pm 0.014 | 0.016 \pm 0.020 | 0.028 \pm 0.025 |

1310

1311 Table 3. Contributions to the rate of change of PET and its radiative and aerodynamic
 1312 components. For each variable, the first column shows the contribution calculated using
 1313 regional averages, along with the associated 95% CI. The second column shows the
 1314 contribution calculated at 1 km resolution, then averaged over each region. The uncertainty on
 1315 this value is difficult to calculate as the pixels are highly spatially correlated, so the
 1316 uncertainty range from the regional analysis is used in Fig. 13.

| a) Contribution to rate of change of PET (mm d ⁻¹ decade ⁻¹) | | | | | | | | | | | | |
|--|------------------------------------|--------|------------------------------------|--------|------------------------------------|--------|-----------------------------------|-------|-----------------------------------|-------|-----------------------------------|-------|
| | Air temperature | | Specific humidity | | Wind speed | | Downward LW | | Downward SW | | Total | |
| | Regional | Pixel | Regional | Pixel | Regional | Pixel | Regional | Pixel | Regional | Pixel | Regional | Pixel |
| England | 0.041 ± 0.025 | 0.039 | -0.025 ± 0.019 | -0.024 | -0.010 ± 0.005 | -0.007 | 0.005 ± 0.006 | 0.005 | 0.013 ± 0.009 | 0.012 | 0.025 ± 0.034 | 0.024 |
| Scotland | 0.029 ± 0.021 | 0.023 | -0.020 ± 0.018 | -0.017 | -0.010 ± 0.005 | -0.007 | 0.006 ± 0.005 | 0.006 | 0.005 ± 0.005 | 0.004 | 0.010 ± 0.029 | 0.008 |
| Wales | 0.039 ± 0.028 | 0.036 | -0.026 ± 0.018 | -0.025 | -0.011 ± 0.007 | -0.009 | 0.006 ± 0.006 | 0.006 | 0.010 ± 0.009 | 0.009 | 0.017 ± 0.036 | 0.017 |
| English lowlands | 0.043 ± 0.029 | 0.042 | -0.024 ± 0.020 | -0.023 | -0.008 ± 0.004 | -0.008 | 0.005 ± 0.006 | 0.005 | 0.015 ± 0.010 | 0.015 | 0.031 ± 0.038 | 0.030 |
| Great Britain | 0.037 ± 0.026 | 0.031 | -0.023 ± 0.018 | -0.022 | -0.010 ± 0.005 | -0.007 | 0.006 ± 0.005 | 0.005 | 0.010 ± 0.007 | 0.007 | 0.019 ± 0.033 | 0.014 |
| b) Contribution to rate of change of radiative component of (mm d ⁻¹ decade ⁻¹) | | | | | | | | | | | | |
| | Air temperature | | Specific humidity | | Wind speed | | Downward LW | | Downward SW | | Total | |
| | Regional | Pixel | Regional | Pixel | Regional | Pixel | Regional | Pixel | Regional | Pixel | Regional | Pixel |
| England | -0.009 ± 0.006 | -0.009 | n/a | n/a | 0.009 ± 0.005 | 0.007 | 0.005 ± 0.006 | 0.005 | 0.014 ± 0.010 | 0.013 | 0.018 ± 0.013 | 0.016 |
| Scotland | -0.006 ± 0.005 | -0.006 | n/a | n/a | 0.009 ± 0.004 | 0.007 | 0.006 ± 0.005 | 0.006 | 0.005 ± 0.005 | 0.004 | 0.014 ± 0.010 | 0.012 |
| Wales | -0.007 ± 0.005 | -0.007 | n/a | n/a | 0.014 ± 0.009 | 0.013 | 0.006 ± 0.006 | 0.006 | 0.010 ± 0.009 | 0.010 | 0.023 ± 0.015 | 0.022 |
| English lowlands | -0.010 ± 0.007 | -0.010 | n/a | n/a | 0.007 ± 0.004 | 0.006 | 0.005 ± 0.006 | 0.005 | 0.016 ± 0.011 | 0.015 | 0.017 ± 0.014 | 0.017 |
| Great Britain | -0.008 ± 0.006 | -0.007 | n/a | n/a | 0.009 ± 0.005 | 0.007 | 0.006 ± 0.006 | 0.006 | 0.010 ± 0.008 | 0.008 | 0.017 ± 0.012 | 0.013 |
| c) Contribution to rate of change of aerodynamic component of PET (mm d ⁻¹ decade ⁻¹) | | | | | | | | | | | | |
| | Air temperature | | Specific humidity | | Wind speed | | Downward LW | | Downward SW | | Total | |
| | Regional | Pixel | Regional | Pixel | Regional | Pixel | Regional | Pixel | Regional | Pixel | Regional | Pixel |

| | | | | | | | | | | | | |
|-------------------------|-----------------------------------|-------|------------------------------------|--------|------------------------------------|--------|-----|-----|-----|-----|----------------------|--------|
| England | 0.052 ± 0.032 | 0.050 | -0.026 ± 0.020 | -0.026 | -0.018 ± 0.010 | -0.015 | n/a | n/a | n/a | n/a | 0.007 ± 0.039 | 0.009 |
| Scotland | 0.037 ± 0.027 | 0.033 | -0.021 ± 0.019 | -0.019 | -0.019 ± 0.010 | -0.015 | n/a | n/a | n/a | n/a | -0.003 ± 0.034 | -0.001 |
| Wales | 0.048 ± 0.035 | 0.046 | -0.028 ± 0.019 | -0.027 | -0.026 ± 0.016 | -0.023 | n/a | n/a | n/a | n/a | -0.005 ± 0.042 | -0.003 |
| England and Wales | 0.056 ± 0.037 | 0.055 | -0.026 ± 0.021 | -0.025 | -0.015 ± 0.008 | -0.014 | n/a | n/a | n/a | n/a | 0.015 ± 0.044 | 0.015 |
| Great Britain | 0.046 ± 0.033 | 0.041 | -0.025 ± 0.019 | -0.023 | -0.020 ± 0.010 | -0.015 | n/a | n/a | n/a | n/a | 0.002 ± 0.039 | 0.003 |

1317
1318

1319 Table 4. Contribution of the trend in each variable to the trends in annual mean PET and its
 1320 radiative and aerodynamic components as a percentage of the fitted trend in PET and its
 1321 components.

| a) Potential evapotranspiration (PET) | | | | | | |
|---------------------------------------|-----------------|-------------------|------------|-------------|-------------|--------|
| | Air temperature | Specific humidity | Wind speed | Downward LW | Downward SW | Total |
| England | 154 % | -88 % | -22 % | 17 % | 47 % | 108 % |
| Scotland | 150 % | -74 % | -23 % | 26 % | 18 % | 97 % |
| Wales | 200 % | -130 % | -38 % | 28 % | 50 % | 109 % |
| English lowlands | 142 % | -77 % | -20 % | 15 % | 45 % | 105 % |
| Great Britain | 155 % | -87 % | -23 % | 19 % | 31 % | 96 % |
| b) Radiative component of PET | | | | | | |
| | Air temperature | Specific humidity | Wind speed | Downward LW | Downward SW | Total |
| England | -47 % | n/a | 40 % | 28 % | 71 % | 92 % |
| Scotland | -42 % | n/a | 62 % | 46 % | 36 % | 102 % |
| Wales | -34 % | n/a | 69 % | 29 % | 52 % | 116 % |
| English lowlands | -53 % | n/a | 35 % | 27 % | 86 % | 95 % |
| Great Britain | -44 % | n/a | 46 % | 31 % | 53 % | 87 % |
| c) Aerodynamic component of PET | | | | | | |
| | Air temperature | Specific humidity | Wind speed | Downward LW | Downward SW | Total |
| England | 245 % | -115 % | -48 % | n/a | n/a | 82 % |
| Scotland | 68 % | -14 % | -33 % | n/a | n/a | 21 % |
| Wales | -135 % | 72 % | -42 % | n/a | n/a | -105 % |
| English lowlands | 282 % | -126 % | -47 % | n/a | n/a | 109 % |
| Great Britain | 168 % | -76 % | -44 % | n/a | n/a | 48 % |

1322
 1323

1324 Table 5. Contributions to the rate of change of PET and its radiative and aerodynamic
 1325 components. For each variable, the first column shows the contribution calculated using
 1326 regional averages, along with the associated 95% CI. The second column shows the
 1327 contribution calculated at 1 km resolution, then averaged over each region. The uncertainty on
 1328 this value is difficult to calculate as the pixels are highly spatially correlated, so the
 1329 uncertainty range from the regional analysis is used in Fig. 13.

| a) Contribution to rate of change of PET ($\text{mm d}^{-1} \text{decade}^{-1}$) | | | | | | | | | | | | |
|---|--|--------|-------------------------|-------|--|--------|---------------------------------------|-------|---------------------------------------|-------|---------------------------------------|-------|
| | Air temperature | | Relative humidity | | Wind speed | | Downward LW | | Downward SW | | Total | |
| | Regional | Pixel | Regional | Pixel | Regional | Pixel | Regional | Pixel | Regional | Pixel | Regional | Pixel |
| England | -0.002 \pm 0.001 | -0.000 | 0.015 \pm 0.016 | 0.013 | -0.010 \pm 0.005 | -0.007 | 0.005 \pm 0.006 | 0.005 | 0.013 \pm 0.009 | 0.012 | 0.021 \pm 0.020 | 0.023 |
| Scotland | -0.001 \pm 0.001 | 0.000 | 0.011 \pm 0.011 | 0.008 | -0.010 \pm 0.005 | -0.007 | 0.006 \pm 0.005 | 0.006 | 0.005 \pm 0.005 | 0.004 | 0.010 \pm 0.014 | 0.011 |
| Wales | -0.002 \pm 0.001 | -0.000 | 0.013 \pm 0.014 | 0.012 | -0.011 \pm 0.007 | -0.009 | 0.006 \pm 0.006 | 0.006 | 0.010 \pm 0.009 | 0.009 | 0.015 \pm 0.019 | 0.018 |
| English lowlands | -0.003 \pm 0.002 | -0.000 | 0.017 \pm 0.018 | 0.017 | -0.008 \pm 0.004 | -0.008 | 0.005 \pm 0.006 | 0.005 | 0.015 \pm 0.010 | 0.015 | 0.026 \pm 0.022 | 0.028 |
| Great Britain | -0.002 \pm 0.001 | 0.000 | 0.013 \pm 0.015 | 0.011 | -0.010 \pm 0.005 | -0.007 | 0.006 \pm 0.005 | 0.005 | 0.010 \pm 0.007 | 0.007 | 0.016 \pm 0.018 | 0.016 |
| b) Contribution to rate of change of radiative component of ($\text{mm d}^{-1} \text{decade}^{-1}$) | | | | | | | | | | | | |
| | Air temperature | | Relative humidity | | Wind speed | | Downward LW | | Downward SW | | Total | |
| | Regional | Pixel | Regional | Pixel | Regional | Pixel | Regional | Pixel | Regional | Pixel | Regional | Pixel |
| England | -0.009 \pm 0.006 | -0.009 | n/a | n/a | 0.009 \pm 0.005 | 0.007 | 0.005 \pm 0.006 | 0.005 | 0.014 \pm 0.010 | 0.013 | 0.018 \pm 0.013 | 0.016 |
| Scotland | -0.006 \pm 0.005 | -0.006 | n/a | n/a | 0.009 \pm 0.004 | 0.007 | 0.006 \pm 0.005 | 0.006 | 0.005 \pm 0.005 | 0.004 | 0.014 \pm 0.010 | 0.012 |
| Wales | -0.007 \pm 0.005 | -0.007 | n/a | n/a | 0.014 \pm 0.009 | 0.013 | 0.006 \pm 0.006 | 0.006 | 0.010 \pm 0.009 | 0.010 | 0.023 \pm 0.015 | 0.022 |
| English lowlands | -0.010 \pm 0.007 | -0.010 | n/a | n/a | 0.007 \pm 0.004 | 0.006 | 0.005 \pm 0.006 | 0.005 | 0.016 \pm 0.011 | 0.015 | 0.017 \pm 0.014 | 0.017 |
| Great Britain | -0.008 \pm 0.006 | -0.007 | n/a | n/a | 0.009 \pm 0.005 | 0.007 | 0.006 \pm 0.006 | 0.006 | 0.010 \pm 0.008 | 0.008 | 0.017 \pm 0.012 | 0.013 |
| c) Contribution to rate of change of aerodynamic component of PET ($\text{mm d}^{-1} \text{decade}^{-1}$) | | | | | | | | | | | | |
| | Air temperature | | Specific humidity | | Wind speed | | Downward LW | | Downward SW | | Total | |
| | Regional | Pixel | Regional | Pixel | Regional | Pixel | Regional | Pixel | Regional | Pixel | Regional | Pixel |

| | | | | | | | | | | | | |
|---------------------|-----------------------------------|-------|---------------------|-------|------------------------------------|--------|-----|-----|-----|-----|----------------------|--------|
| England | 0.006 ± 0.004 | 0.006 | 0.015 ± 0.017 | 0.014 | -0.018 ± 0.010 | -0.015 | n/a | n/a | n/a | n/a | 0.003 ± 0.020 | 0.004 |
| Scotland | 0.004 ± 0.003 | 0.004 | 0.011 ± 0.011 | 0.009 | -0.019 ± 0.010 | -0.015 | n/a | n/a | n/a | n/a | -0.004 ± 0.015 | -0.002 |
| Wales | 0.005 ± 0.004 | 0.005 | 0.013 ± 0.015 | 0.012 | -0.026 ± 0.016 | -0.023 | n/a | n/a | n/a | n/a | -0.007 ± 0.022 | -0.006 |
| English lowlands | 0.007 ± 0.004 | 0.006 | 0.018 ± 0.019 | 0.017 | -0.015 ± 0.008 | -0.014 | n/a | n/a | n/a | n/a | 0.009 ± 0.021 | 0.010 |
| Great Britain | 0.005 ± 0.004 | 0.005 | 0.014 ± 0.015 | 0.011 | -0.020 ± 0.010 | -0.015 | n/a | n/a | n/a | n/a | -0.001 ± 0.019 | 0.000 |

1330
1331

1332 Table 6. Contribution of the trend in each variable to the trends in annual mean PET and its
 1333 radiative and aerodynamic components as a percentage of the fitted trend in PET and its
 1334 components when relative humidity is used.

| a) Potential evapotranspiration (PET) | | | | | | |
|---------------------------------------|-----------------|-------------------|------------|-------------|-------------|-------|
| | Air temperature | Relative humidity | Wind speed | Downward LW | Downward SW | Total |
| England | -0% | 57% | -22% | 17% | 47% | 99% |
| Scotland | 0% | 65% | -23% | 26% | 18% | 85% |
| Wales | -0% | 68% | -38% | 27% | 50% | 107% |
| English lowlands | -0% | 57% | -20% | 15% | 45% | 97% |
| Great Britain | 0% | 60% | -23% | 19% | 31% | 87% |
| b) Radiative component of PET | | | | | | |
| | Air temperature | Relative humidity | Wind speed | Downward LW | Downward SW | Total |
| England | -47% | n/a | 40% | 28% | 71% | 92% |
| Scotland | -42% | n/a | 62% | 46% | 36% | 102% |
| Wales | -34% | n/a | 69% | 29% | 52% | 116% |
| English lowlands | -53% | n/a | 35% | 27% | 86% | 95% |
| Great Britain | -44% | n/a | 46% | 31% | 53% | 87% |
| c) Aerodynamic component of PET | | | | | | |
| | Air temperature | Relative humidity | Wind speed | Downward LW | Downward SW | Total |
| England | 29% | 78% | -48% | n/a | n/a | 59% |
| Scotland | 8% | 14% | -33% | n/a | n/a | -11% |
| Wales | -15% | -33% | -42% | n/a | n/a | -90% |
| English lowlands | 33% | 98% | -47% | n/a | n/a | 84% |
| Great Britain | 19% | 52% | -44% | n/a | n/a | 27% |

1335
 1336

1337 Table A1. Details of sites used for validation of meteorological data.

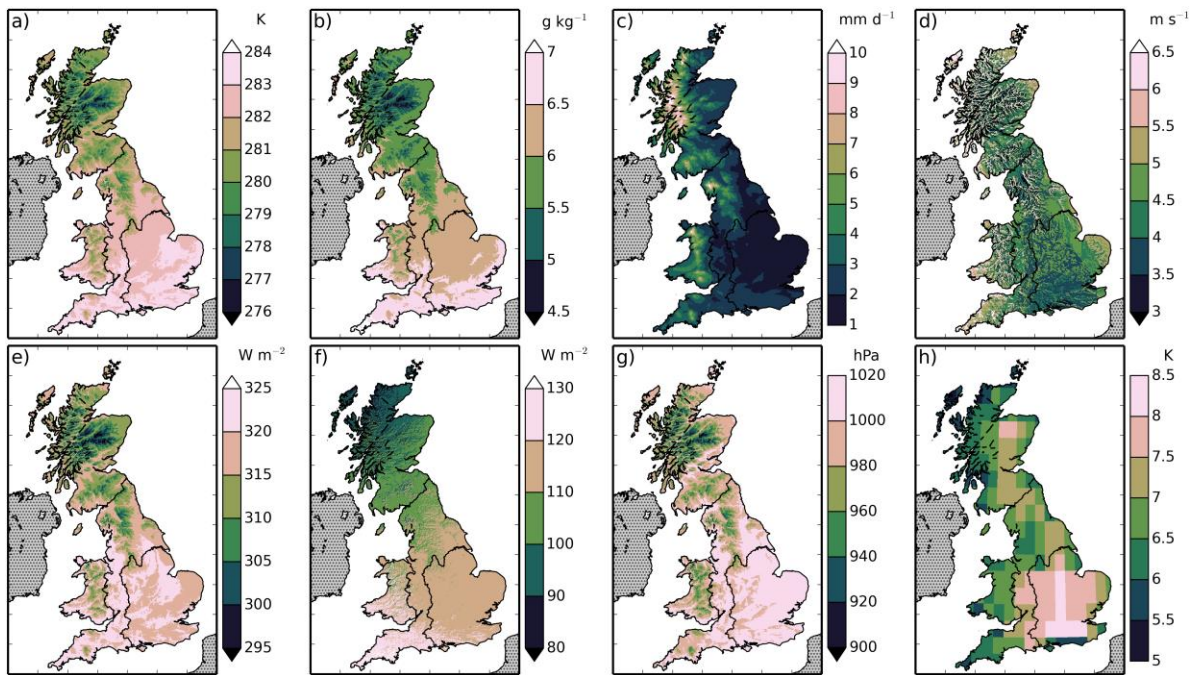
| Site (ID) | Latitude | Longitude | Years | Land cover | Citation |
|---------------------------|----------|-----------|----------------------|-------------------------------|---|
| Alice Holt (UK-Ham) | 51.15 | -0.86 | 2004-2012 | Deciduous broadleaf woodland | (Wilkinson et al., 2012; Heinemeyer et al., 2012) |
| Griffin Forest (UK-Gri) | 56.61 | -3.80 | 1997-2001, 2004-2008 | Evergreen needleleaf woodland | (Clement, 2003) |
| Auchencorth Moss (UK-AMo) | 55.79 | -3.24 | 2002-2006 | Grass and crop | (Billett et al., 2004) |
| Easter Bush (UK-EBu) | 55.87 | -3.21 | 2004-2008 | Grass | (Gilmanov et al., 2007; Soussana et al., 2007) |

1338

1339 Table A2. Correlation statistics for meteorological variables with data from four sites.

| a) Air temperature | | | |
|--------------------------|-------|------------------------------|-----------------------------|
| Site | r^2 | Mean bias | RMSE |
| Alice Holt | 0.95 | 0.10 K | 1.17 K |
| Griffin Forest | 0.94 | 0.21 K | 1.17 K |
| Auchencorth Moss | 0.98 | -0.02 K | 0.78 K |
| Easter Bush | 0.97 | -0.46 K | 0.96 K |
| b) Downward SW radiation | | | |
| Site | r^2 | Mean bias | RMSE |
| Alice Holt | 0.94 | -3.01 W m ⁻² | 22.92 W m ⁻² |
| Griffin Forest | 0.85 | -4.90 W m ⁻² | 31.29 W m ⁻² |
| Auchencorth Moss | 0.91 | 14.27 W m ⁻² | 27.96 W m ⁻² |
| Easter Bush | 0.88 | 5.73 W m ⁻² | 27.15 W m ⁻² |
| c) Mixing ratio | | | |
| Site | r^2 | Mean bias | RMSE |
| Alice Holt | 0.90 | -0.02 mmol mol ⁻¹ | 1.09 mmol mol ⁻¹ |
| Griffin Forest | 0.76 | 0.08 mmol mol ⁻¹ | 1.56 mmol mol ⁻¹ |
| d) Wind speed | | | |
| Site | r^2 | mean bias | RMSE |
| Alice Holt | 0.88 | 1.24 m s ⁻¹ | 1.45 m s ⁻¹ |
| Griffin Forest | 0.59 | 1.36 m s ⁻¹ | 1.81 m s ⁻¹ |
| Auchencorth Moss | 0.63 | -0.38 m s ⁻¹ | 1.37 m s ⁻¹ |
| Easter Bush | 0.82 | 0.44 m s ⁻¹ | 1.03 m s ⁻¹ |
| e) Surface air pressure | | | |
| Site | r^2 | Mean bias | RMSE |
| Griffin Forest | 0.05 | -0.42 hPa | 1.38 hPa |
| Auchencorth Moss | 0.01 | -1.06 hPa | 1.57 hPa |
| Easter Bush | 0.03 | 0.01 hPa | 1.33 hPa |

1340



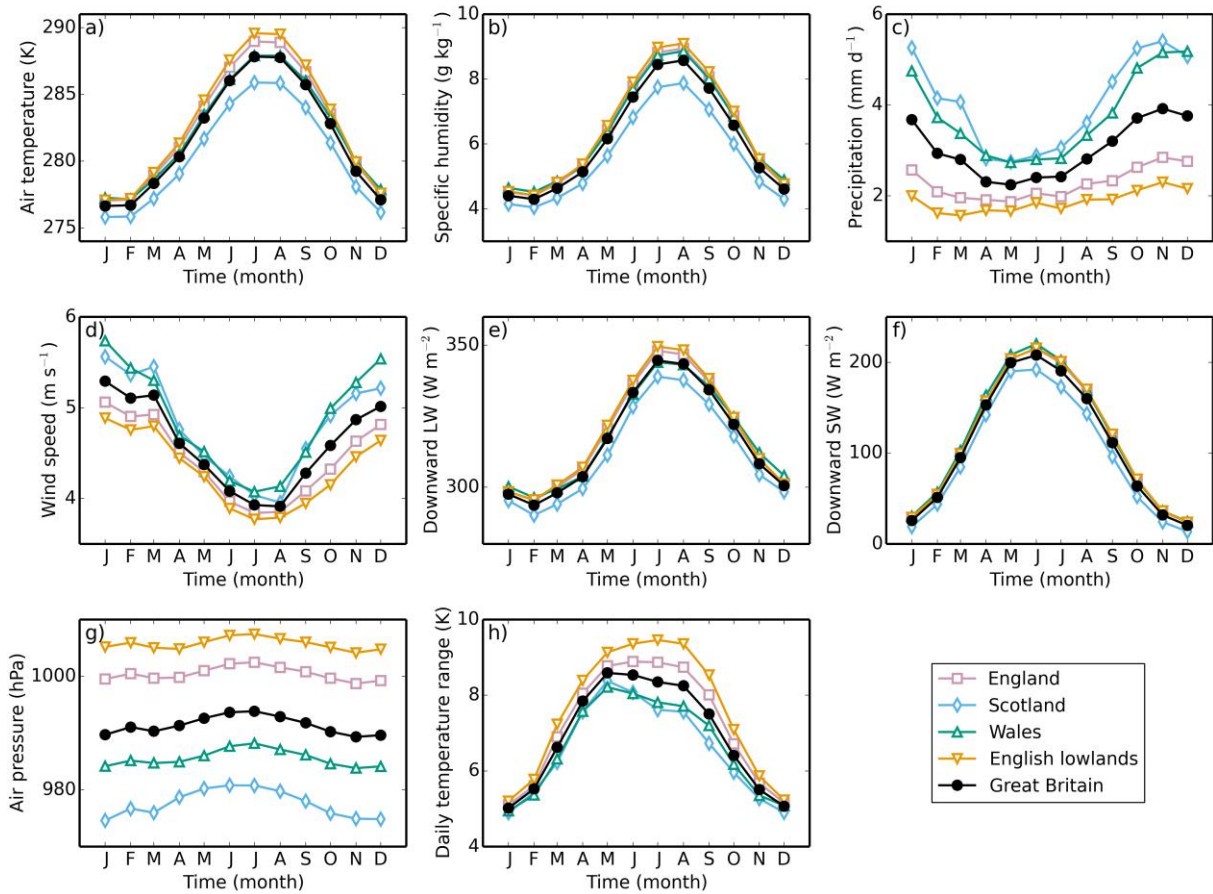
1341

1342 Figure 1. Means of the meteorological variables over the years 1961-2012. The variables are
 1343 a) 1.2 m air temperature, b) 1.2 m specific humidity, c) precipitation, d) 10 m wind speed, e)
 1344 downward LW radiation, f) downward SW radiation, g) surface air pressure, h) daily air
 1345 temperature range.



1346

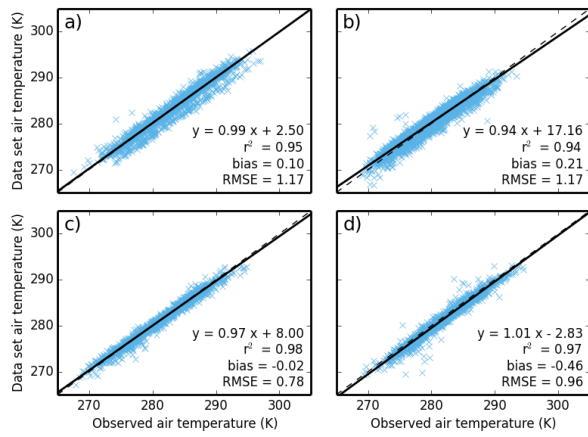
1347 Figure 2. The regions used to calculate the area means. The English lowlands are a sub-region
1348 of England. England, Scotland and Wales together form the fifth region, Great Britain.



1349

1350 Figure 3. Mean monthly climatology of meteorological variables, a) 1.2 m air temperature, b)
 1351 1.2 m specific humidity, c) precipitation, d) 10 m wind speed, e) downward LW radiation, f)
 1352 downward SW radiation, g) surface air pressure, h) daily air temperature range, for five
 1353 different regions of Great Britain, calculated over the years 1961-2012.

1354

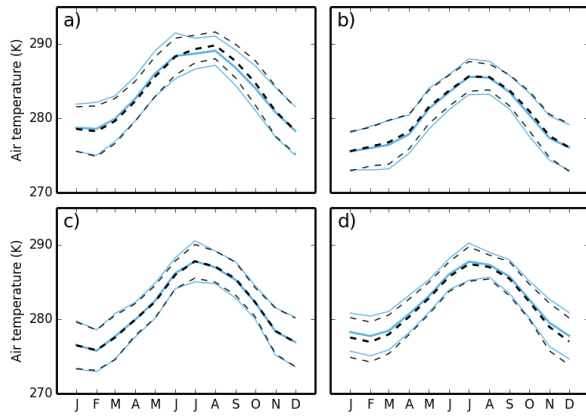


1355

1356 Figure 4. Plot of data set air temperature against daily mean observed air temperature at four
 1357 sites. The dashed line shows the one to one line, while the solid line shows the linear regression,
 1358 the equation of which is shown in the lower right of each plot, along with the r^2 value, the mean
 1359 bias and the RMSE. The sites are a) Alice Holt; b) Griffin Forest; c) Auchencorth Moss; d)
 1360 Easter Bush.

1361

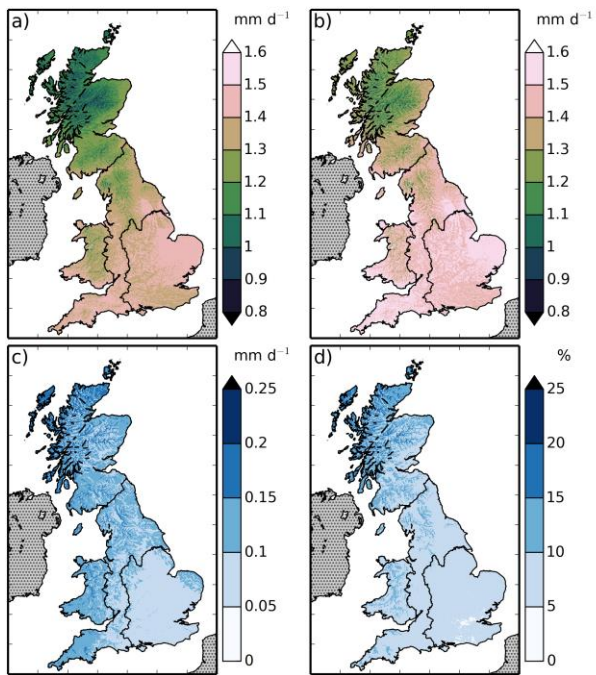
1362



1363

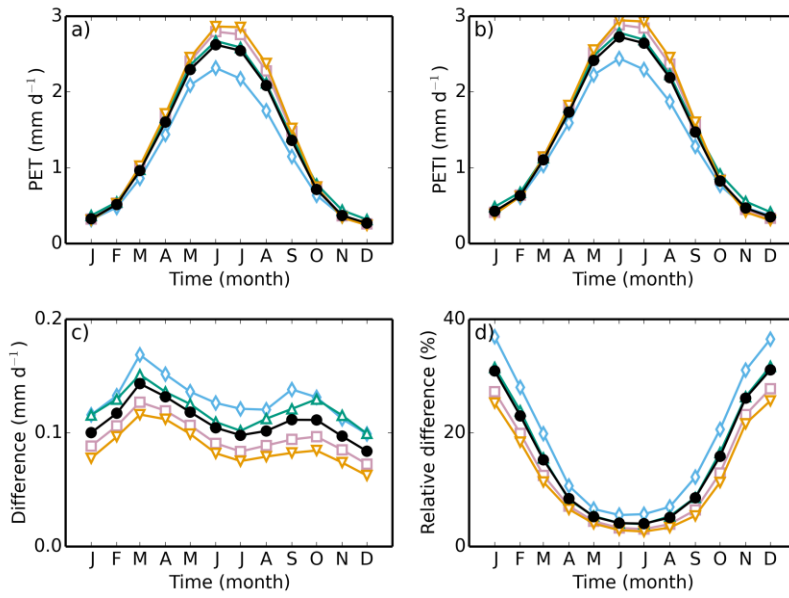
1364 Figure 5. Mean monthly climatology of the dataset (black, dashed lines) and observed (blue,
1365 solid lines) air temperatures, calculated for the period of observations. The thicker lines show
1366 the means, while the thinner lines show the standard errors on each measurement. Sites as in
1367 Fig. 4.

1368



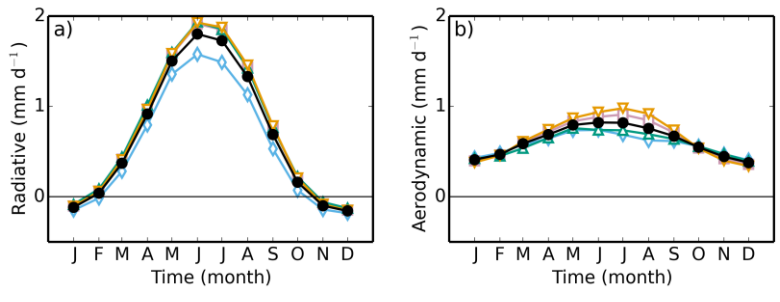
1369

1370 Figure 6. Mean a) PET, b) PETI, c) absolute difference between PETI and PET and d) relative
 1371 difference calculated over the years 1961-2012.



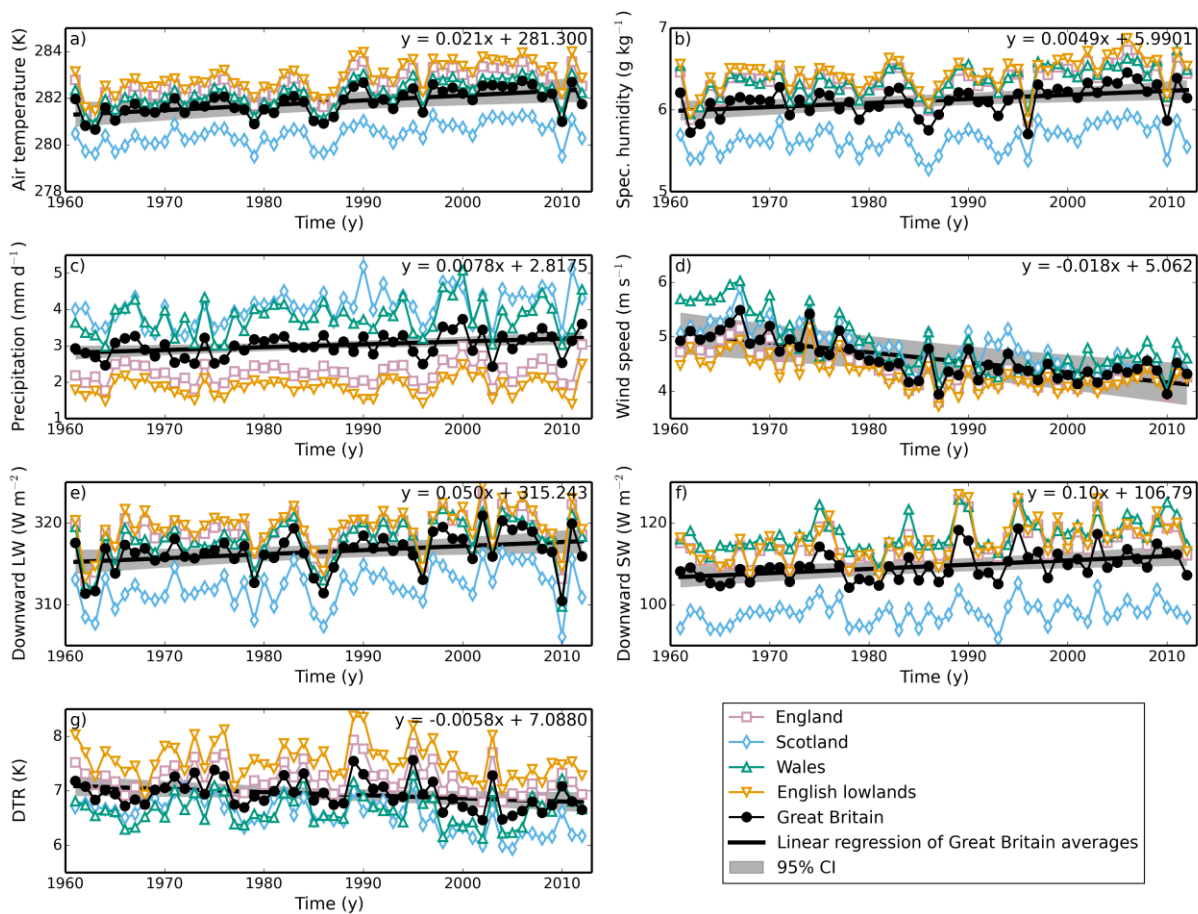
1372

1373 Figure 7. Mean monthly climatology of a) PET, b) PETI, c) absolute difference between PETI
 1374 and PET, d) relative difference, for five different regions of Great Britain, calculated over the
 1375 years 1961-2012. Symbols as in Fig. 3.



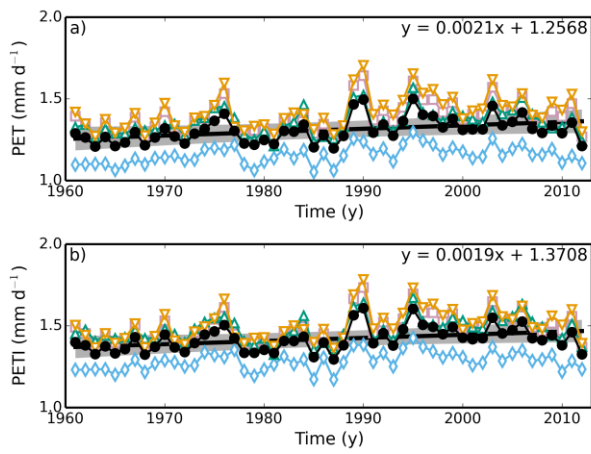
1376

1377 Figure 8. Mean-monthly climatology of the a) radiative and b) aerodynamic components of the
 1378 PET for five different regions of Great Britain, calculated over the years 1961-2012. Symbols
 1379 as in Fig. 3.



1380

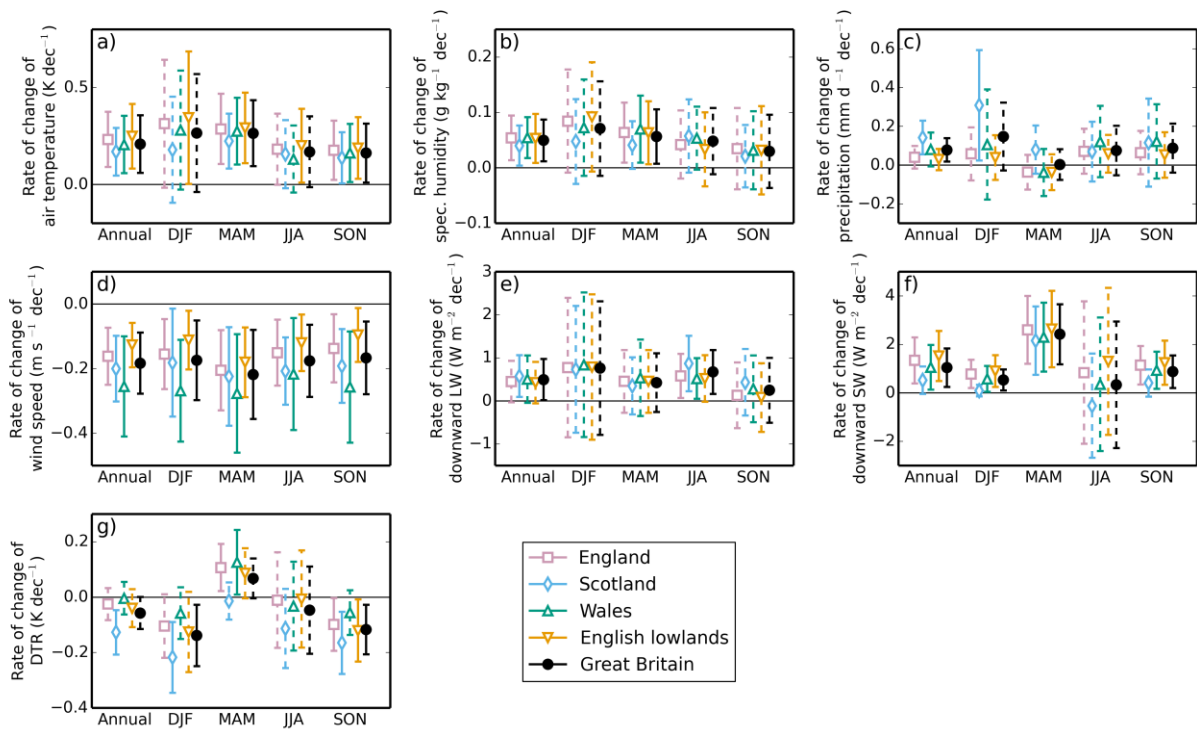
1381 Figure 9. Annual means of the meteorological variables, a) 1.2 m air temperature, b) 1.2 m
 1382 specific humidity, c) precipitation, d) 10 m wind speed, e) downward LW radiation, f)
 1383 downward SW radiation, g) daily air temperature range, over five regions of Great Britain. The
 1384 solid black lines show the linear regression fit to the Great Britain annual means, while the grey
 1385 strip shows the 95% CI of the same fit, assuming a non-zero lag-1 correlation coefficient. The
 1386 equation of this fit is shown in the top right-hand corner of each plot.



1387

1388 Figure 10. Annual means of a) PET and b) PETI for five regions of Great Britain. Symbols as
 1389 in Fig. 9.

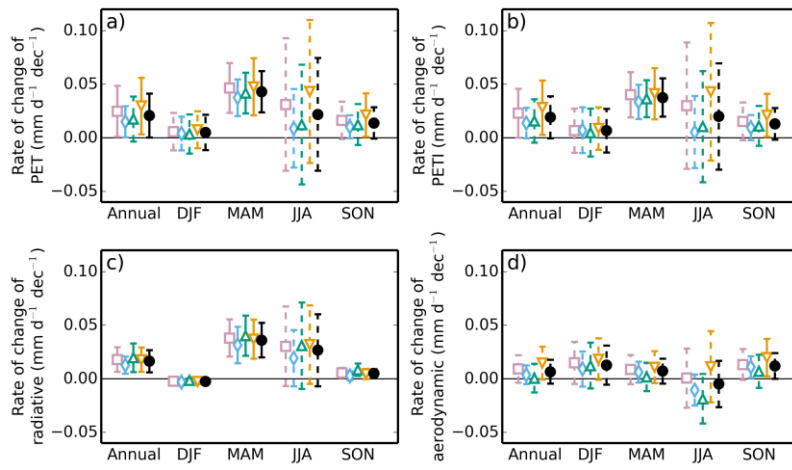
1390



1391

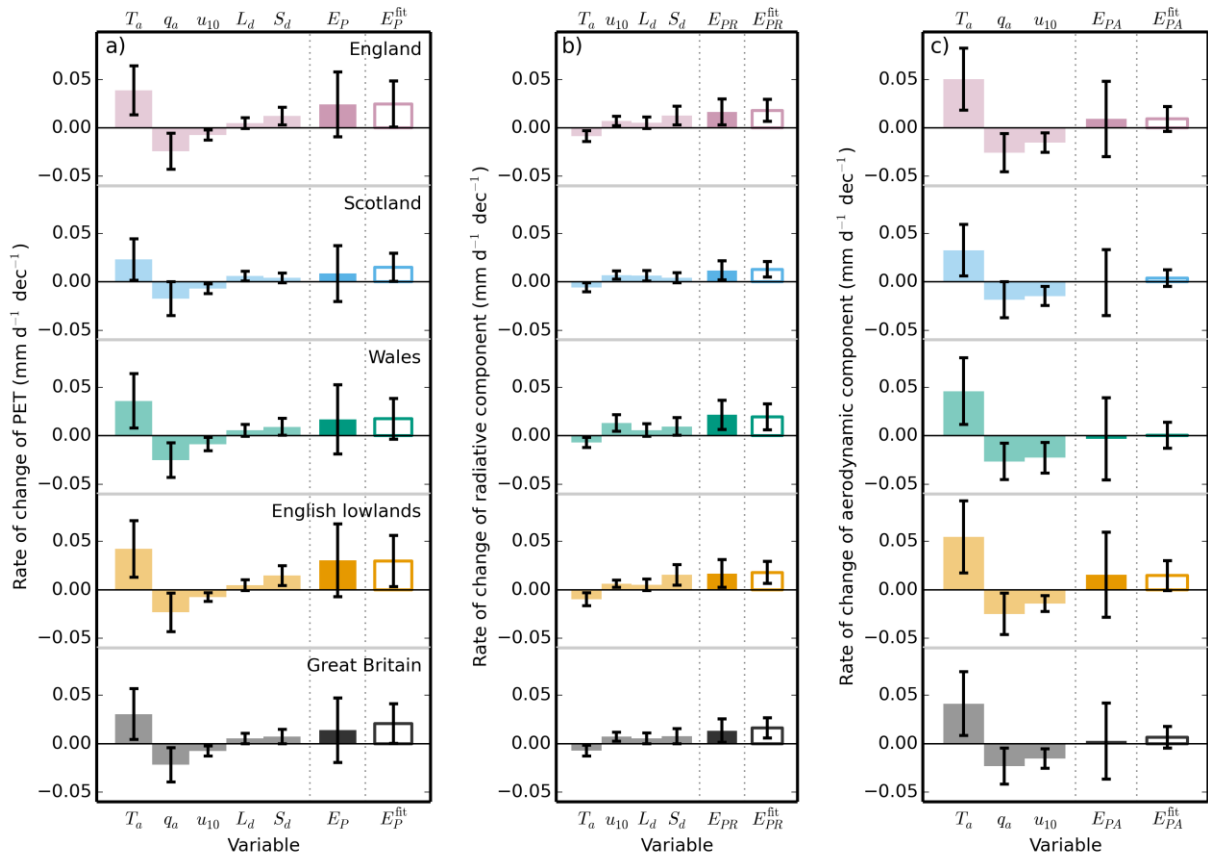
1392 Figure 11. Rate of change of annual and seasonal means of meteorological variables, a) 1.2 m
 1393 air temperature, b) 1.2 m specific humidity, c) precipitation, d) 10 m wind speed, e) downward
 1394 LW radiation, f) downward SW radiation, g) daily air temperature range, for five regions of
 1395 Great Britain for the years 1961-2012. Error bars are the 95% CI calculated assuming a non-
 1396 zero lag-1 correlation coefficient. Solid error bars indicate slopes that are statistically significant
 1397 at the 5% level, dashed error bars indicate slopes that are not significant at the 5% level.

1398



1399

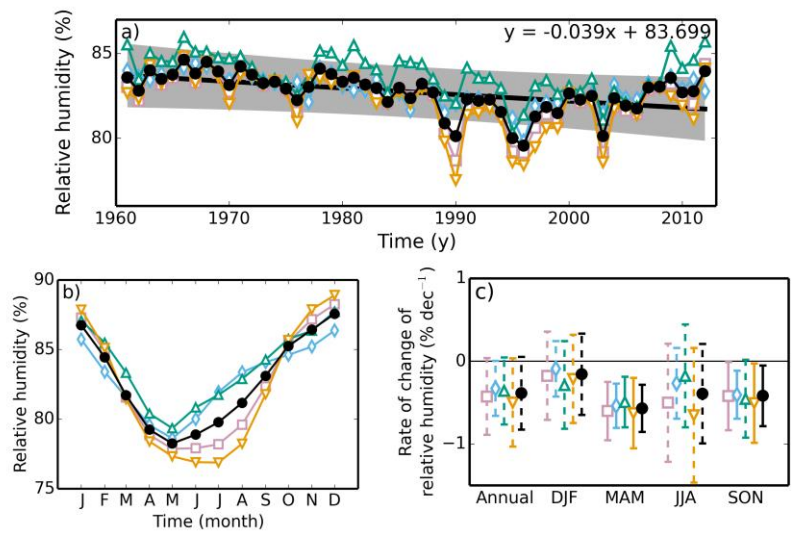
1400 Figure 12. Rate of change of annual and seasonal means of a) PET, b) PETI, c) the radiative
 1401 component of PET and d) the aerodynamic component of PET for five regions of Great Britain
 1402 for the years 1961-2012. Symbols as in Fig. 11.



1403

1404 Figure 13. The contribution of the rate of change of each meteorological variable to the rate of
 1405 change of a) PET, b) the radiative component and c) the aerodynamic component. The first five
 1406 (four; three) bars are the contribution to the rate of change of annual mean PET from the rate
 1407 of change of each of the variables, calculated per pixel, than averaged over each region. Each
 1408 bar has an error bar showing the 95% CI on each value. Since the pixels are highly spatially
 1409 correlated, we use the more conservative CI calculated by applying this analysis to the regional
 1410 means. The next bar is the sum of the other bars and shows the attributed rate of change of
 1411 annual mean PET. The final bar shows the slope and its associated CI obtained from the linear
 1412 regression of the mean annual PET for each region.

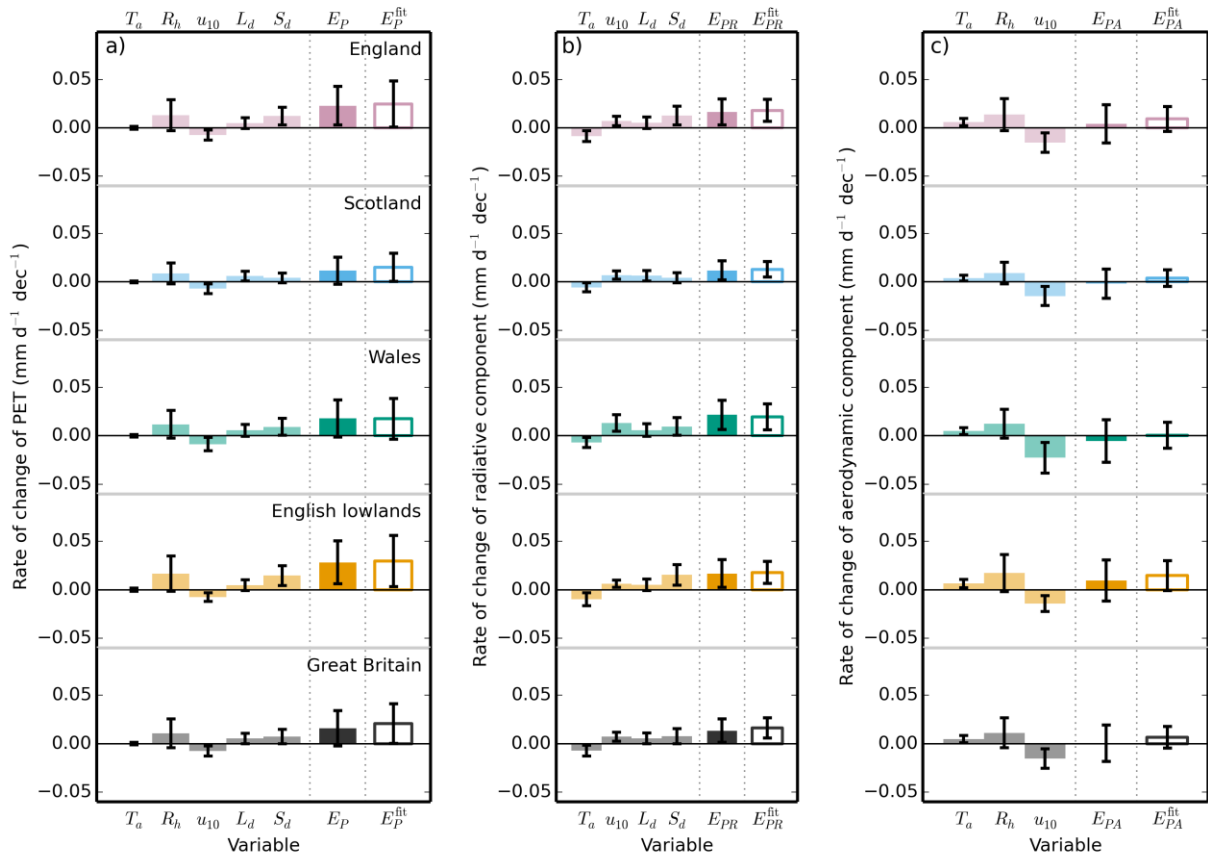
1413



1414

1415 Figure 14. Regional annual means (a), regional mean-monthly climatology (b) and regional
 1416 rates of change of relative humidity for the years 1961-2012.

1417

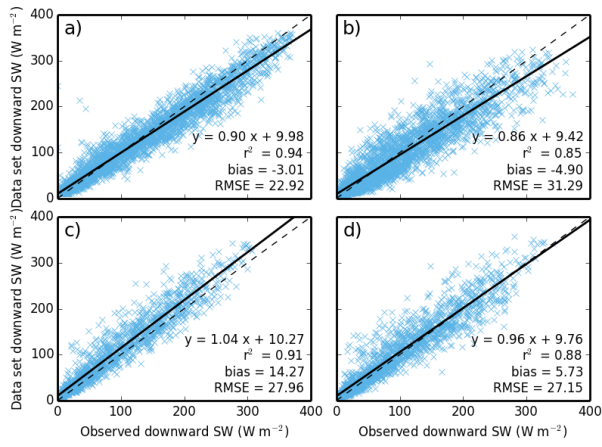


1418

1419 Figure 15. The contribution of the rate of change of each meteorological variable to the rate of
 1420 change of a) PET, b) the radiative component and c) the aerodynamic component, with relative
 1421 humidity instead of specific humidity. The first five (four; three) bars are the contribution to
 1422 the rate of change of annual mean PET from the rate of change of each of the variables,
 1423 calculated per pixel, than averaged over each region. Each bar has an error bar showing the
 1424 95% CI on each value. Since the pixels are highly spatially correlated, we use the more
 1425 conservative CI calculated by applying this analysis to the regional means. The next bar is the
 1426 sum of the other bars and shows the attributed rate of change of annual mean PET. The final
 1427 bar shows the slope and its associated CI obtained from the linear regression of the mean annual
 1428 PET for each region.

1429

1430



1431

1432

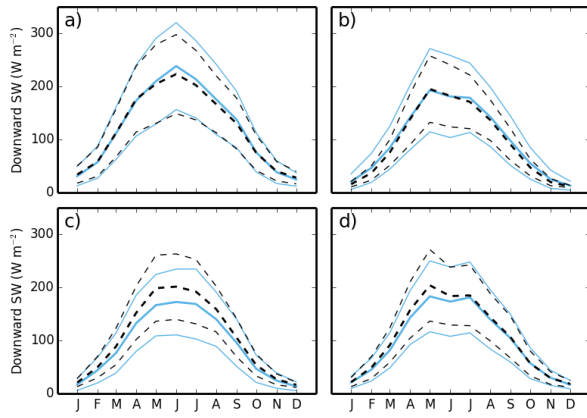
Figure A1. Plot of data set downward SW radiation against daily mean observed downward

1433

SW radiation at four flux sites. Symbols and sites as in Fig. 4.

1434

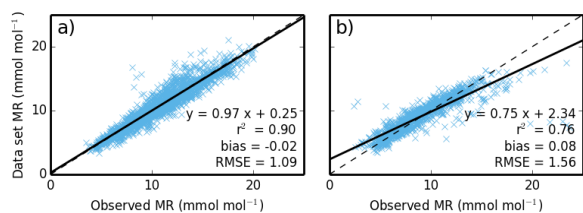
1435



1436

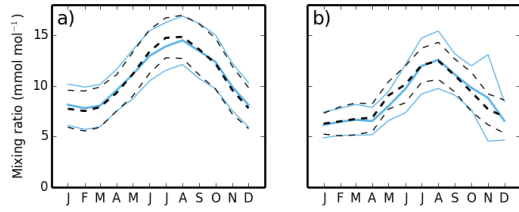
1437 Figure A2. Mean monthly climatology of the dataset (black, dashed lines) and observed (blue,
1438 solid lines) downward SW radiation, calculated for the period of observations. Symbols as in
1439 Fig. 5, sites as in Fig. 4.

1440



1441
 1442 Figure A3. Plot of mixing ratio calculated using dataset meteorology against daily mean
 1443 observed mixing ratio at four sites. Symbols as in Fig. 4. The sites are a) Alice Holt and b)
 1444 Griffin Forest.
 1445

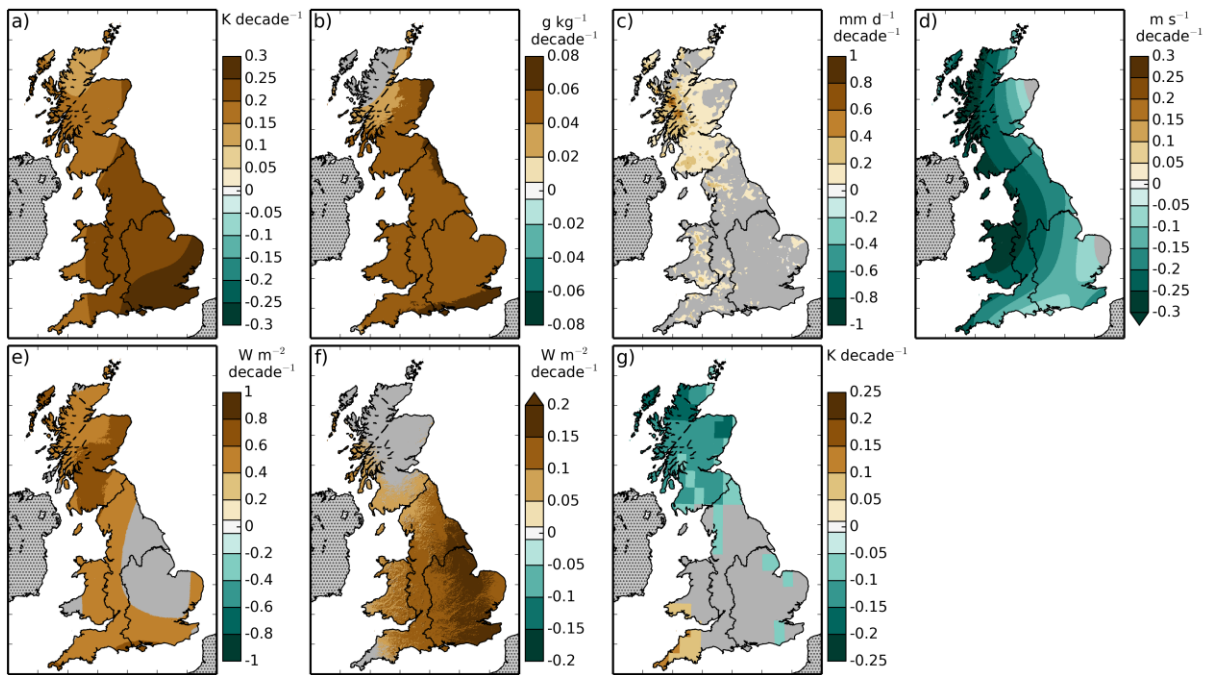
1446



1447

1448 Figure A4. Mean monthly climatology of the dataset (black, dashed lines) and observed (blue,
1449 solid lines) mixing ratio, calculated for the period of observations. Symbols as in Fig. 5. Sites
1450 as in Fig. A3.

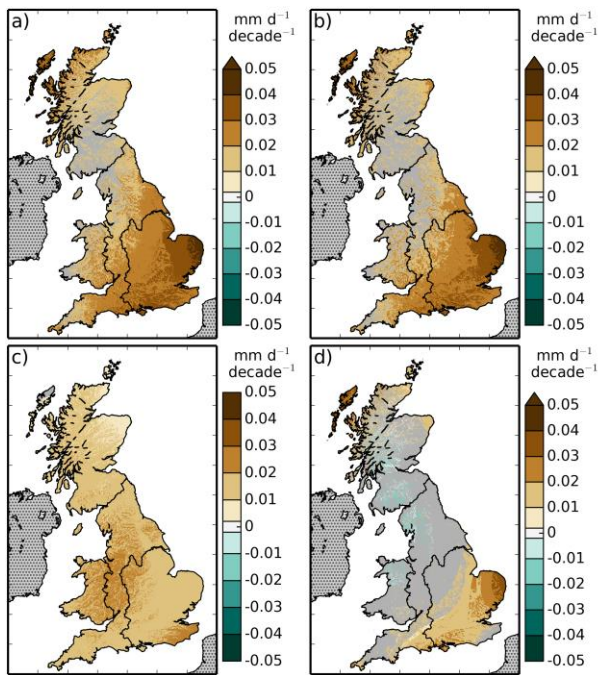
1451



1452

1453 Figure B1. Rate of change of the annual means of the meteorological variables, a) 1.2 m air
 1454 temperature, b) 1.2 m specific humidity, c) precipitation, d) 10 m wind speed, e) downward LW
 1455 radiation, f) downward SW radiation, g) daily air temperature range over the period 1961-2012.
 1456 Areas for which the trend was not significant are shown in grey.

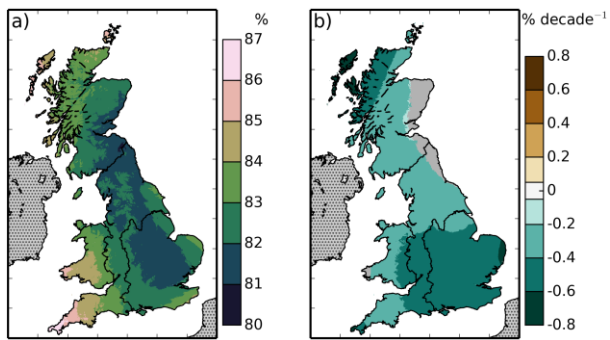
1457



1458

1459 Figure B2. Rate of change the annual means of a) PET, b) PETI, c) the radiative component of
 1460 PET, d) the aerodynamic component of PET over the period 1961-2012. Areas for which the
 1461 trend was not significant are shown in grey.

1462



1463

1464 Figure B3. Mean of the relative humidity over the years 1961-2012 (a). Rate of change of the
 1465 annual mean of relative humidity (b). Areas for which the trend was not significant are shown
 1466 in grey.

1467